

1 The X-linked intellectual disability gene KDM5C is a
2 sex-biased brake against germline programs in somatic
3 lineages

4

5 Katherine M. Bonefas^{1,2}, Ilakkiya Venkatachalam^{2,3}, and Shigeki Iwase².

6 1. Neuroscience Graduate Program, University of Michigan Medical School, Ann Arbor, MI, 48109, USA.

7 2. Department of Human Genetics, Michigan Medicine, University of Michigan Medical School, Ann Arbor,
8 MI, 48109, USA.

9 3. Genetics and Genomics Graduate Program, University of Michigan, Ann Arbor, MI, 48109, USA.

10 Correspondence should be addressed to K. Bonefas and S. Iwase (siwase@umich.edu)

11 Abstract

12 Mutations in numerous chromatin-modifying enzymes cause neurodevelopmental disorders (NDDs). Loss
13 of repressive chromatin regulators can lead to the aberrant transcription of tissue-specific genes outside
14 of their intended context, however the mechanisms and consequences of their dysregulation are largely
15 unknown. Here, we examine how the X-linked intellectual disability gene lysine demethylase 5c (KDM5C), an
16 eraser of histone 3 lysine 4 di and tri-methylation (H3K4me2/3), contributes to tissue identity. We found male
17 *Kdm5c* knockout (-KO) mice, which recapitulate key human neurological phenotypes, aberrantly express
18 many liver, muscle, ovary, and testis genes within the amygdala and hippocampus. Gonad-enriched genes
19 misexpressed in the *Kdm5c*-KO brain are unique to germ cells, indicating an erosion of the soma-germline
20 boundary. Germline genes are typically decommissioned in somatic lineages in the post-implantation epiblast,
21 yet *Kdm5c*-KO epiblast-like cells (EpiLCs) aberrantly expressed key regulators of germline identity and
22 meiosis, including *Dazl* and *Stra8*. Characterizing germline gene misexpression in males and female mutants
23 revealed germline gene repression is sexually dimorphic, with female EpiLCs requiring a higher dose of
24 KDM5C to maintain germline gene suppression. Using a comprehensive list of mouse germline-enriched
25 genes, we found KDM5C is selectively recruited to a subset of germline gene promoters that contain CpG
26 islands (CGIs) to facilitate DNA CpG methylation during ESC to EpiLC differentiation. However, late-stage
27 spermatogenesis genes devoid of promoter CGIs can become expressed in *Kdm5c*-KO cells via ectopic
28 activation by RFX transcription factors. Together, these data demonstrate KDM5C's fundamental role in
29 tissue identity and indicate that KDM5C acts as a brake against runaway activation of germline developmental
30 programs in somatic lineages.

31 Introduction

32 A single genome holds the instructions to generate the myriad of cell types found within an organism.
33 This is, in part, accomplished by chromatin regulators that can either promote or impede lineage-specific
34 gene expression through DNA and histone modifications^{1–5}. Human genetic studies revealed mutations in
35 chromatin regulators are a major cause of neurodevelopmental disorders (NDDs)⁶ and many studies have
36 identified their importance for regulating brain-specific transcriptional programs. Loss of chromatin regulators
37 can also result in the ectopic expression of tissue-specific genes outside of their target environment, such
38 as the misexpression of liver-specific genes within adult neurons⁷. However, the mechanisms underlying
39 ectopic gene expression and its impact upon neurodevelopment are poorly understood.

40 To elucidate the role of tissue identity in chromatin-linked NDDs, it is essential to first characterize the
41 nature of the dysregulated genes and the molecular mechanisms governing their de-repression. Here we
42 focus on the X chromosome gene lysine demethylase 5C (KDM5C, also known as SMCX or JARID1C),
43 which erases histone 3 lysine 4 di- and trimethylation (H3K4me2/3), a permissive chromatin modification
44 enriched at gene promoters⁸. Pathogenic mutations in *KDM5C* cause Intellectual Developmental Disorder,
45 X-linked, Syndromic, Claes-Jensen Type (MRXSCJ, OMIM: 300534). MRXSCJ is more common and severe
46 in males and its neurological phenotypes include intellectual disability, seizures, aberrant aggression, and
47 autistic behaviors^{9–11}. Male *Kdm5c* knockout (-KO) mice recapitulate key MRXSCJ phenotypes, including
48 hyperaggression, increased seizure propensity, social deficits, and learning impairments^{12–14}. RNA sequenc-
49 ing (RNA-seq) of the *Kdm5c*-KO hippocampus revealed ectopic expression of some germline genes within
50 the brain¹³. However, it is unclear if other tissue-specific genes are aberrantly transcribed with KDM5C loss,
51 at what point in development germline gene misexpression begins, and what mechanisms underlie their
52 dysregulation.

53 Distinguishing between germ cells and somatic cells is a key feature of multicellularity¹⁵ that occurs
54 during early embryogenesis in many metazoans¹⁶. In mammals, chromatin regulators are crucial for
55 decommissioning germline genes during the transition from naïve to primed pluripotency. Initially, germline
56 gene promoters gain repressive histone H2A lysine 119 monoubiquitination (H2AK119ub1)¹⁷ and histone H3
57 lysine 9 trimethylation (H3K9me3)^{17,18} in embryonic stem cells (ESCs) and are then decorated with DNA
58 CpG methylation (CpGme) in post-implantation epiblast cells^{18–21}. The contribution of KDM5C to this process
59 remains unclear. Additionally, studies on germline gene repression have primarily been conducted in males
60 and focused on select marker genes, given the lack of a comprehensive list for germline-enriched genes.
61 Therefore, it is unknown if the mechanism of repression differs between sexes or for different classes of
62 germline genes, e.g. meiotic versus spermatid differentiation genes.

63 To illuminate KDM5C's role in tissue identity, here we characterized the aberrant expression of tissue-
64 enriched genes within the *Kdm5c*-KO brain and epiblast-like stem cells (EpiLCs), an *in vitro* model of the
65 post-implantation embryo. We curated a list of mouse germline-enriched genes, which enabled genome-wide

66 analysis of germline gene silencing mechanisms for the first time. Additionally, we characterized germline
67 transcripts expressed in male and female *Kdm5c* mutants to illuminate the impact of sex upon germline
68 gene suppression. Based on the data presented below, we propose KDM5C plays a fundamental, sexually
69 dimorphic role in the development of tissue identity during early embryogenesis, including the establishment
70 of the soma-germline boundary.

71 **Results**

72 **Tissue-enriched genes are aberrantly expressed in the *Kdm5c*-KO brain**

73 Previous RNA sequencing (RNA-seq) of the adult male *Kdm5c*-KO hippocampus revealed ectopic
74 expression of some germline genes unique to the testis¹³. It is currently unknown if the testis is the only
75 tissue type misexpressed in the *Kdm5c*-KO brain. We thus systematically tested whether other tissue-specific
76 genes are misexpressed in the male brain with constitutive knockout of *Kdm5c* (*Kdm5c*^{-y}, 5CKO in figures)²²
77 by using a published list of mouse tissue-enriched genes²³.

78 We found a large proportion of significantly upregulated genes (DESeq2²⁴, log2 fold change > 0.5, q <
79 0.1) within the male *Kdm5c*-KO amygdala and hippocampus are non-brain, tissue-specific genes (Amygdala:
80 0/0 up DEGs, NaN% ; Hippocampus: 0/0 up DEGs, NaN%) (Figure 1A-B, Supplementary Table 1). For both
81 the amygdala and hippocampus, the majority of tissue-enriched differentially expressed genes (DEGs) were
82 testis genes (Figure 1A-B). Even though the testis has the largest total number of tissue-enriched genes
83 (2,496 genes) compared to any other tissue, testis-enriched DEGs were significantly enriched in both brain
84 regions (Amygdala p = 1.83e-05, Odds Ratio = 5.13; Hippocampus p = 4.26e-11, Odds Ratio = 4.45, Fisher's
85 Exact Test). An example of a testis-enriched gene misexpressed in the *Kdm5c*-KO brain is *FK506 binding*
86 *protein 6 (Fkbp6)*, a known regulator of PIWI-interacting RNAs (piRNAs) and meiosis^{25,26} (Figure 1C).

87 Interestingly, we also observed significant enrichment of ovary-enriched genes in both the amygdala
88 and hippocampus (Amygdala p = 0.00574, Odds Ratio = 18.7; Hippocampus p = 0.048, Odds Ratio = 5.88,
89 Fisher's Exact Test) (Figure 1A-B). Ovary-enriched DEGs included *Zygotic arrest 1 (Zar1)*, which sequesters
90 mRNAs in oocytes for meiotic maturation²⁷ (Figure 1D). Given that the *Kdm5c*-KO mice we analyzed are
91 male, these data demonstrate that the ectopic expression of gonad-enriched genes is independent of
92 organismal sex.

93 Although not consistent across brain regions, we also found significant enrichment of genes biased
94 towards two non-gonadal tissues - the liver (Amygdala p = 0.04, Odds Ratio = 6.58, Fisher's Exact Test)
95 and muscle (Hippocampus p = 0.01, Odds Ratio = 6.95, Fisher's Exact Test) (Figure 1A-B). These include
96 *Apolipoprotein C-I (Apoc1)*, a lipoprotein metabolism and transport gene²⁸ (Figure 1E, see Discussion).

97 Our analysis of oligo(dT)-primed libraries²² indicates aberrantly expressed mRNAs are polyadenylated
98 and spliced into mature transcripts in the *Kdm5c*-KO brain (Figure 1C-E). Of note, we observed little to no

99 dysregulation of brain-enriched genes (Amygdala p = 1, Odds Ratio = 1.22; Hippocampus p = 0.74, Odds
100 Ratio = 1.22, Fisher's Exact Test), despite the fact these are brain samples and the brain has the second
101 highest total number of tissue-enriched genes (708 genes). Altogether, these results suggest the aberrant
102 expression of tissue-enriched genes within the brain is a major effect of KDM5C loss.

103 **Germline genes are misexpressed in the *Kdm5c*-KO brain**

104 *Kdm5c*-KO brain expresses testicular germline genes¹³ (Figure 1), however the testis also contains
105 somatic cells that support hormone production and germline functions. To determine if *Kdm5c*-KO results
106 in ectopic expression of testicular somatic genes, we first evaluated the known functions of testicular
107 DEGs through gene ontology. We found *Kdm5c*-KO testis-enriched DEGs had high enrichment of germline-
108 relevant ontologies, including spermatid development (GO: 0007286, p.adjust = 6.2e-12) and sperm axoneme
109 assembly (GO: 0007288, p.adjust = 2.45e-14) (Figure 2A, Supplementary Table 1).

110 We then evaluated *Kdm5c*-KO testicular DEG expression in wild-type testes versus testes with germ cell
111 depletion²⁹, which was accomplished by heterozygous *W* and *Wv* mutations in the enzymatic domain of *c-Kit*
112 (*Kit*^{W/Wv})³⁰. Almost all *Kdm5c*-KO testis-enriched DEGs lost expression with germ cell depletion (Figure 2B).
113 We then assessed testis-enriched DEG expression in a published single cell RNA-seq dataset that identified
114 cell type-specific markers within the testis³¹. Some *Kdm5c*-KO testis-enriched DEGs were classified as
115 specific markers for different germ cell developmental stages (e.g. spermatogonia, spermatocytes, round
116 spermatids, and elongating spermatids), yet none marked somatic cells (Figure 2C). Together, these data
117 demonstrate that the *Kdm5c*-KO brain aberrantly expresses germline genes but not somatic testicular genes,
118 reflecting an erosion of the soma-germline boundary.

119 As of yet, research on germline gene silencing mechanisms has focused on a handful of key genes rather
120 than assessing germline gene suppression genome-wide, due to the lack of a comprehensive gene list.
121 We therefore generated a list of mouse germline-enriched genes using RNA-seq datasets of *Kit*^{W/Wv} mice
122 that included males and females at embryonic day 12, 14, and 16³² and adult male testes²⁹. We defined
123 genes as germline-enriched if their expression met the following criteria: 1) their expression is greater than
124 1 FPKM in wild-type gonads 2) their expression in any non-gonadal tissue of adult wild type mice²³ does
125 not exceed 20% of their maximum expression in the wild-type germline, and 3) their expression in the germ
126 cell-depleted gonads, for any sex or time point, does not exceed 20% of their maximum expression in the
127 wild-type germline. These criteria yielded 1,288 germline-enriched genes (Figure 2D), which was hereafter
128 used as a resource to globally characterize germline gene misexpression with *Kdm5c* loss (Supplementary
129 Table 2).

130 ***Kdm5c*-KO epiblast-like cells aberrantly express key regulators of germline identity**

131 Germ cells are typically distinguished from somatic cells soon after the embryo implants into the uterine
132 wall^{33,34}, when germline genes are silenced in epiblast stem cells that will form the somatic tissues³⁵. This
133 developmental time point can be modeled *in vitro* through differentiation of naïve embryonic stem cells
134 (nESCs) into epiblast-like stem cells (EpiLCs) (Figure 3A)^{36,37}. While some germline-enriched genes are
135 also expressed in nESCs and in the 2-cell stage^{38–40}, they are silenced as they differentiate into EpiLCs^{18,19}.
136 Therefore, we tested if KDM5C was necessary for the initial silencing of germline genes in somatic lineages
137 by evaluating the impact of *Kdm5c* loss in male EpiLCs.

138 *Kdm5c*-KO cell morphology during ESC to EpiLC differentiation appeared normal (Figure 3B) and EpiLCs
139 properly expressed markers of primed pluripotency, such as *Dnmt3b*, *Fgf5*, *Pou3f1*, and *Otx2* (Figure 3C). We
140 then identified tissue-enriched DEGs in a RNA-seq dataset of wild-type and *Kdm5c*-KO EpiLCs⁴¹ (DESeq2,
141 log₂ fold change > 0.5, q < 0.1, Supplementary Table 3). Similar to the *Kdm5c*-KO brain, we observed
142 general dysregulation of tissue-enriched genes, with the largest number of genes belonging to the brain and
143 testis, although they were not significantly enriched (Figure 3D). Using our list of mouse germline-enriched
144 genes assembled above, we identified 68 germline genes misexpressed in male *Kdm5c*-KO EpiLCs.

145 We then compared EpiLC germline DEGs to those expressed in the *Kdm5c*-KO brain to determine if
146 germline genes are constitutively dysregulated or change over the course of development. The majority of
147 germline DEGs were unique to either EpiLCs or the brain, with only *D1Pas1* and *Cyct* shared across all
148 tissue/cell types (Figure 3E-F). EpiLC germline DEGs had particularly high enrichment of meiosis-related
149 gene ontologies when compared to the brain (Figure 3G, Supplementary Table 3), such as meiotic cell
150 cycle process (GO:1903046, p.adjust = 2.2e-07) and meiotic nuclear division (GO:0140013, p.adjust
151 = 1.37e-07). While there was modest enrichment of meiotic gene ontologies in both brain regions, the
152 *Kdm5c*-KO hippocampus primarily expressed late-stage spermatogenesis genes involved in sperm axoneme
153 assembly (GO:0007288, p.adjust = 0.00621) and sperm motility (GO:0097722, p.adjust = 0.00612).

154 Notably, DEGs unique to *Kdm5c*-KO EpiLCs included key drivers of germline identity, such as *Stimulated*
155 *by retinoic acid 8* (*Stra8*: log₂ fold change = 3.73, q = 2.17e-39) and *Deleted in azoospermia like* (*Dazl*:
156 log₂ fold change = 3.36, q = 3.19e-12) (Figure 3H). These genes are typically expressed when a subset
157 of epiblast stem cells become primordial germ cells (PGCs) and then again in mature germ cells to trigger
158 meiotic gene expression programs^{42–44}. Of note, some germline genes, including *Dazl*, are also expressed
159 in the two-cell embryo^{39,45}. However, we did not see derepression of two-cell stage-specific genes, like
160 *Duxf3* (*Dux*) (log₂ fold change = -0.282, q = 0.337) and *Zscan4d* (log₂ fold change = 0.25, q = 0.381) (Figure
161 3H, Supplementary Table 3), indicating *Kdm5c*-KO EpiLCs do not revert back to a 2-cell state. Altogether,
162 *Kdm5c*-KO EpiLCs express key drivers of germline identity and meiosis while the brain primarily expresses
163 spermiogenesis genes, indicating germline gene misexpression mirrors germline development during the
164 progression of somatic development.

165 **Female epiblast-like cells have heightened germline gene misexpression with *Kdm5c***
166 **loss**

167 It is currently unknown if the misexpression of germline genes is influenced by sex, as previous studies
168 on germline gene repressors have focused on male cells^{17,18,20,46,47}. Sex is particularly pertinent in the case
169 of KDM5C because it partially escapes X chromosome inactivation (XCI), resulting in a higher dosage in
170 females^{48–51}. We therefore explored the impact of chromosomal sex upon germline gene suppression by
171 comparing their dysregulation in male *Kdm5c* hemizygous knockout (*Kdm5c*^{-y}, XY *Kdm5c*-KO, XY 5CKO),
172 female homozygous knockout (*Kdm5c*^{-/-}, XX *Kdm5c*-KO, XX 5CKO), and female heterozygous knockout
173 (*Kdm5c*^{-/+}, XX *Kdm5c*-HET, XX 5CHET) EpiLCs⁴¹.

174 In EpiLCs, homozygous and heterozygous *Kdm5c* knockout females expressed over double the number
175 of germline-enriched genes than hemizygous males (Figure 4A, Supplementary Table 3). While the majority
176 of germline DEGs in *Kdm5c*-KO males were also dysregulated in females (74%), many were sex-specific,
177 such as *Tktl2* and *Esx1* (Figure 4B). We then compared the known functions of germline genes dysregulated
178 uniquely in males and females or misexpressed in all samples (Figure 4C, Supplementary Table 3). Female-
179 specific germline DEGs were enriched for meiotic (GO:0051321 - meiotic cell cycle, p.adjust = 7.81E-14) and
180 flagellar (GO:0003341 - cilium movement, p.adjust = 4.87E-06) functions, while male-specific DEGs had roles
181 in mitochondrial and cell signaling (GO:0070585 - protein localization to mitochondrion, p.adjust = 0.025).

182 The majority of germline genes expressed in both sexes were more highly dysregulated in females
183 compared to males (Figure 4D-F). This increased degree of dysregulation in females, along with the
184 increased total number of germline genes, indicates females are more sensitive to losing KDM5C-mediated
185 germline gene suppression. Heightened germline gene dysregulation in females could be due to impaired
186 XCI in *Kdm5c* mutants⁴¹, as many spermatogenesis genes lie on the X chromosome^{52,53}. However, female
187 germline DEGs were not biased towards the X chromosome (p = 1, Odds Ratio = 0.96, Fisher's Exact Test)
188 and females had a similar overall proportion of germline DEGs belonging to the X chromosome as males
189 (XY *Kdm5c*-KO - 10.29%, XX *Kdm5c*-HET - 7.43%, XX *Kdm5c*-KO - 10.59%) (Figure 4G). The majority of
190 germline DEGs instead lie on autosomes for both male and female *Kdm5c* mutants (Figure 4G). Thus, while
191 female EpiLCs are more prone to germline gene misexpression with KDM5C loss, it is likely independent of
192 XCI defects.

193 **Germline gene misexpression in *Kdm5c* mutants is independent of germ cell sex**

194 Although many germline genes have shared functions in the male and female germline, e.g. PGC
195 formation, meiosis, and genome defense, some have unique or sex-biased expression. Therefore, we
196 wondered if *Kdm5c* mutant males would primarily express sperm genes while mutant females would primarily
197 express egg genes. To comprehensively assess whether germline gene sex corresponds with *Kdm5c*
198 mutant sex, we first filtered our list of germline-enriched genes for egg and sperm-biased genes (Figure 4,

199 Supplementary Table 2). We defined germ cell sex-biased genes as those whose expression in the opposite
200 sex, at any time point, is no greater than 20% of the gene's maximum expression in a given sex. This
201 criteria yielded 67 egg-biased, 1,024 sperm-biased, and 197 unbiased germline-enriched genes. We found
202 regardless of sex, egg, sperm, and unbiased germline genes were dysregulated in all *Kdm5c* mutants at
203 similar proportions (Figure 4I-J). Furthermore, germline genes dysregulated exclusively in either male or
204 female mutants were also not biased towards their corresponding germ cell sex (Figure 4I). Altogether, these
205 results demonstrate sex differences in germline gene dysregulation is not due to sex-specific activation of
206 sperm or egg transcriptional programs.

207 KDM5C binds to a subset of germline gene promoters during early embryogenesis

208 KDM5C binds to the promoters of several germline genes in embryonic stem cells (ESCs) but not in
209 neurons^{13,54}. However, due to the lack of a comprehensive list of germline-enriched genes, it is unclear if
210 KDM5C is enriched at germline gene promoters, what types of germline genes KDM5C regulates, and if its
211 binding is maintained at any germline genes in neurons.

212 To address these questions, we analyzed KDM5C chromatin immunoprecipitation followed by DNA
213 sequencing (ChIP-seq) datasets in EpiLCs⁴¹ and primary forebrain neuron cultures (PNCs)¹² (MACS2 q <
214 0.1, fold enrichment > 1, and removal of false-positive *Kdm5c*-KO peaks). EpiLCs had a higher total number
215 of high-confidence KDM5C peaks than PNCs (EpiLCs: 5,808, PNCs: 1,276). KDM5C was primarily localized
216 to gene promoters in both cell types (promoters = transcription start site (TSS) ± 500 bp, EpiLCs: 4,190,
217 PNCs: 745), although PNCs showed increased localization to non-promoter regions (Figure 5A).

218 The majority of promoters bound by KDM5C in PNCs were also bound in EpiLCs (513 shared promoters),
219 however a large portion of gene promoters were bound by KDM5C only in EpiLCs (3,677 EpiLC only
220 promoters) (Figure 5B). Genes bound by KDM5C in both PNCs and EpiLCs were enriched for functions
221 involving nucleic acid turnover, such as deoxyribonucleotide metabolic process (GO:0009262, p.adjust =
222 8.28e-05) (Figure 5C, Supplementary Table 4). Germline ontologies were enriched only in EpiLC-specific,
223 KDM5C-bound promoters, such as meiotic nuclear division (GO: 0007127 p.adjust = 6.77e-16) (Figure 5C).
224 There were no significant ontologies for PNC-specific KDM5C target genes. Using our mouse germline gene
225 list, we observed evident KDM5C signal around the TSS of many germline genes in EpiLCs, but not in PNCs
226 (Figure 5D). Based on our ChIP-seq peak cut-off criteria, KDM5C was highly enriched at 211 germline gene
227 promoters in EpiLCs (16.4% of all germline genes) (Figure 5E, Supplementary Table 2). Of note, KDM5C
228 was only bound to about one third of RNA-seq DEG promoters unique to EpiLCs or the brain (EpiLC only
229 DEGs: 34.9%, Brain only DEGs: 30%) (Supplementary Figure 1A-C). Representative examples of EpiLC
230 DEGs bound and unbound by KDM5C in EpiLCs are *Dazl* and *Stra8*, respectively (Figure 5F). However,
231 the four of the five germline genes dysregulated in both EpiLCs and the brain were bound by KDM5C in
232 EpiLCs (*D1Pas1*, *Hsf2bp*, *Cyct*, and *Stk31*) (Supplementary Figure 1A). Together, these results demonstrate
233 KDM5C is recruited to a subset of germline genes in EpiLCs, including meiotic genes, but does not directly

234 regulate germline genes in neurons. Furthermore, the majority of germline mRNAs expressed in *Kdm5c*-KO
235 cells are dysregulated independent of direct KDM5C recruitment to their gene promoters, however genes
236 dysregulated across *Kdm5c*-KO development are often direct KDM5C targets.

237 Many germline-specific genes are suppressed by the polycomb repressive complex 1.6 (PRC1.6), which
238 contains the transcription factor heterodimers E2F/DP1 and MGA/MAX that respectively bind E2F and
239 E-box motifs within germline gene promoters^{17,18,20,40,46,47,55-57}. PRC1.6 members may recruit KDM5C to
240 germline gene promoters¹³, given their association with KDM5C in HeLa cells and ESCs^{45,58}. We thus
241 used HOMER⁵⁹ to identify transcription factor motifs enriched at KDM5C-bound or unbound germline gene
242 promoters (TSS ± 500 bp, q-value < 0.1, Supplementary Table 4). MAX and E2F6 binding sites were
243 significantly enriched at germline genes bound by KDM5C in EpiLCs (MAX q-value: 0.0068, E2F6 q-value:
244 0.0673, E2F q-value: 0.0917), but not at germline genes unbound by KDM5C (Figure 5G). One third of
245 KDM5C-bound promoters contained the consensus sequence for either E2F6 (E2F, 5'-TCCCGC-3'), MGA
246 (E-box, 5'-CACGTG-3'), or both, but only 17% of KDM5C-unbound genes contained these motifs (Figure 5H).
247 KDM5C-unbound germline genes were instead enriched for multiple RFX transcription factor binding sites
248 (RFX q-value < 0.0001, RFX2 q-value < 0.0001, RFX5 q-value < 0.0001) (Figure 5I, Supplementary figure
249 1D). RFX transcription factors bind X-box motifs⁶⁰ to promote ciliogenesis^{61,62} and among them is RFX2, a
250 central regulator of post-meiotic spermatogenesis^{63,64}. Although *Rfx2* is also not a direct target of KDM5C
251 (Supplementary Figure 1E), RFX2 mRNA is derepressed in *Kdm5c*-KO EpiLCs (Figure 5J). Thus, RFX2 is a
252 candidate transcription factor for driving the ectopic expression of many KDM5C-unbound germline genes in
253 *Kdm5c*-KO cells.

254 **KDM5C is recruited to CpG islands at germline promoters to facilitate *de novo* DNA
255 methylation**

256 Previous work found two germline gene promoters have a marked reduction in DNA CpG methylation
257 (CpGme) in the adult *Kdm5c*-KO hippocampus¹³. Since histone H3K4me2/3 impede *de novo* CpGme^{65,66},
258 KDM5C's removal of H3K4me2/3 may be required to suppress germline genes. However, KDM5C's catalytic
259 activity was recently shown to be dispensable for suppressing *Dazl* in undifferentiated ESCs⁴⁵. To reconcile
260 these observations, we hypothesized KDM5C erases H3K4me2/3 to promote the initial placement of CpGme
261 at germline gene promoters in EpiLCs.

262 To test this hypothesis, we first characterized KDM5C's expression as naïve ESCs differentiate into
263 EpiLCs (Figure 6A). While *Kdm5c* mRNA steadily decreased from 0 to 48 hours of differentiation (Figure
264 6B), KDM5C protein initially increased from 0 to 24 hours and then decreased to near knockout levels by 48
265 hours (Figure 6C). We then characterized KDM5C's substrates (H3K4me2/3) at germline gene promoters
266 with *Kdm5c* loss using published ChIP-seq datasets^{22,41}. *Kdm5c*-KO samples showed a marked increase in
267 H3K4me2 in EpiLCs (Figure 6D) and H3K4me3 in the amygdala (Figure 6E) around the TSS of germline

268 genes. Together, these data suggest KDM5C acts during the transition between ESCs and EpiLCs to remove
269 H3K4me2/3 at germline gene promoters.

270 Germline genes accumulate CpG methylation (CpGme) at CpG islands (CGIs) during the transition
271 from naïve to primed pluripotency^{19,21,67}. We first examined how many of our germline-enriched genes had
272 promoter CGIs (TSS ± 500 bp) using the UCSC genome browser⁶⁸. Notably, out of 1,288 germline-enriched
273 genes, only 356 (27.64%) had promoter CGIs (Figure 6F, Supplementary Table 2). CGI-containing germline
274 genes had higher enrichment of meiotic gene ontologies compared to CGI-free genes, including meiotic
275 nuclear division (GO:0140013, p.adjust = 2.17e-12) and meiosis I (GO:0007127, p.adjust = 3.91e-10)
276 (Figure 6G, Supplementary Table 5). Germline genes with promoter CGIs were more highly expressed than
277 CGI-free genes across spermatogenesis stages, with highest expression in meiotic spermatocytes (Figure
278 6H). Contrastingly, CGI-free genes only displayed substantial expression in post-meiotic round spermatids
279 (Figure 6H). Although only a minor portion of germline gene promoters contained CGIs, CGIs strongly
280 determined KDM5C's recruitment to germline genes ($p = 2.37e-67$, Odds Ratio = 17.8, Fisher's Exact Test),
281 with 79.15% of KDM5C-bound germline gene promoters harboring CGIs (Figure 6F).

282 To assess how KDM5C loss impacts initial CpGme placement at germline gene promoters, we performed
283 whole genome bisulfite sequencing (WGBS) in male wild-type and *Kdm5c*-KO ESCs and 96-hour extend
284 EpiLCs (exEpiLCs), when germline genes reach peak methylation levels¹⁸ (Figure 6I). We first identified
285 which germline gene promoters significantly gained CpGme in wild-type cells during nESC to exEpiLCs
286 differentiation (methylKit⁶⁹, $q < 0.01$, $|methylation\ difference| > 25\%$, TSS ± 500 bp). In wild-type cells, the
287 majority of germline genes gained substantial CpGme at their promoter during differentiation (60.08%),
288 regardless if their promoter contained a CGI (Figure 6J, Supplementary Table 5).

289 We then identified promoters differentially methylated in wild-type versus *Kdm5c*-KO exEpiLCs (methylKit,
290 $q < 0.01$, $|methylation\ difference| > 25\%$, TSS ± 500 bp, Supplementary Table 5). Of the 48,882 promoters
291 assessed, 274 promoters were significantly hypomethylated and 377 promoters were significantly hyper-
292 methylated with KDM5C loss (Supplementary Figure 2A). Many promoters hyper- and hypomethylated
293 in *Kdm5c*-KO exEpiLCs belonged to genes with unknown functions. However, 10.22% of hypomethyl-
294 ated promoters belonged to germline genes and germline-relevant ontologies like meiotic nuclear division
295 (GO:0140013, p.adjust = 0.012) are significantly enriched (Supplementary Figure 2B, Supplementary Table
296 5). Approximately half of all germline gene promoters hypomethylated in *Kdm5c*-KO exEpiLCs are direct
297 targets of KDM5C in EpiLCs (13 out of 28 hypomethylated promoters).

298 Promoters that showed the most robust loss of CpGme in *Kdm5c*-KO exEpiLCs (lowest q-values) harbored
299 CGIs (Figure 6K). CGI promoters, but not CGI-free promoters, had a significant reduction in CpGme with
300 KDM5C loss as a whole (Figure 6L) (Non-CGI promoters $p = 0.0846$, CGI promoters $p = 0.0081$, Mann-
301 Whitney U test). Significantly hypomethylated promoters included germline genes consistently dysregulated
302 across multiple *Kdm5c*-KO RNA-seq datasets¹³, such as *D1Pas1* (methylation difference = -60.03%, q-value
303 = 3.26e-153) and *Naa11* (methylation difference = -42.45%, q-value = 1.44e-38) (Figure 6M). Unexpectedly,

304 we observed only a modest reduction in CpGme at *Dazl*'s promoter (methylation difference = -6.525%,
305 q-value = 0.0159) (Figure 6N). Altogether, these results demonstrate KDM5C is recruited to germline gene
306 CGIs in EpiLCs to promote CpGme at those promoters. Furthermore, our data suggest while KDM5C's
307 catalytic activity is required for the repression of some germline genes, CpGme can be placed at others even
308 with elevated H3K4me2/3 around the TSS.

309 Discussion

310 In the above study, we demonstrate KDM5C's pivotal role in the development of tissue identity. We first
311 characterized tissue-enriched genes expressed within the mouse *Kdm5c*-KO brain and identified substantial
312 derepression of testis, liver, muscle, and ovary-enriched genes. Testis genes significantly enriched within the
313 *Kdm5c*-KO amygdala and hippocampus are specific to the germline and absent in somatic cells. *Kdm5c*-
314 KO epiblast-like cells (EpiLCs) aberrantly express key drivers of germline identity and meiosis, including
315 *Dazl* and *Stra8*, while the adult brain primarily expresses genes important for late spermatogenesis. We
316 demonstrated that although sex did not influence whether sperm or egg-specific genes were misexpressed,
317 female EpiLCs have heightened germline gene de-repression with KDM5C loss. Germline genes can become
318 aberrantly expressed in *Kdm5c*-KO cells via indirect mechanisms, such as activation through ectopic RFX
319 transcription factors. Finally, we found KDM5C is dynamically regulated during ESC to EpiLC differentiation
320 to promote long-term germline gene silencing through CGI DNA methylation. Therefore, we propose KDM5C
321 plays a fundamental role in the development of tissue identity during early embryogenesis, including the
322 establishment of the soma-germline boundary. By systematically characterizing KDM5C's role in germline
323 gene repression, we unveiled distinct mechanisms governing the misexpression of distinct germline gene
324 classes in somatic lineages. Ultimately, these data provide molecular footholds which can be exploited to
325 test the overarching contribution of ectopic germline gene expression upon neurodevelopment.

326 By comparing *Kdm5c* mutant males and females, we revealed germline gene suppression is sexually
327 dimorphic. Female EpiLCs are more severely impacted by loss of KDM5C-mediated germline gene sup-
328 pression, yet this difference is not due to the large number of germline genes on the X chromosome^{52,53}.
329 Heightened germline gene misexpression in females may be related to females having a higher dose of
330 KDM5C than males, due to its escape from XCI^{48–51}. Intriguingly, heterozygous knockout females (*Kdm5c*^{-/+})
331 also had over double the number of germline DEGs than hemizygous knockout males (*Kdm5c*^{-/Y}), even
332 though their expression of KDM5C should be roughly equivalent to that of wild-type males (*Kdm5c*^{+/Y}). Males
333 could partially compensate for KDM5C's loss via the Y-chromosome homolog, KDM5D⁸. However, KDM5D
334 has not been reported to regulate germline gene expression. Nevertheless, these results demonstrate
335 germline gene silencing mechanisms differ between males and females, which warrants further study to
336 elucidate the biological ramifications and underlying mechanisms.

337 We found KDM5C is largely dispensable for promoting normal gene expression during development, yet

338 is critical for suppressing ectopic developmental programs. While some germline genes, such as *Dazl*, are
339 also expressed in the 2-cell stage, the inner cell mass, and naïve ESCs, they are silenced in epiblast stem
340 cells/EpiLCs^{18,40,45,70,71}. Our data suggest the 2-cell-like state reported in *Kdm5c*-KO ESCs⁴⁵ likely reflects
341 KDM5C's primary role in germline gene repression (Figure 3). Germline gene misexpression in *Kdm5c*-
342 KO EpiLCs may indicate they are differentiating into primordial germ cell-like cells (PGCLCs)^{33,34,36}. Yet,
343 *Kdm5c*-KO EpiLCs had normal cellular morphology and properly expressed markers for primed pluripotency,
344 including *Otx2* which blocks EpiLC differentiation into PGCs/PGCLCs⁷². In addition to unimpaired EpiLC
345 differentiation, *Kdm5c*-KO gross brain morphology is overall normal¹² and hardly any brain-specific genes
346 were significantly dysregulated in the amygdala and hippocampus (Figure 1). Thus, ectopic germline gene
347 expression occurs in conjunction with overall proper somatic differentiation in *Kdm5c*-KO animals.

348 Our work provides novel insight into the cross-talk between H3K4me2/3 and CpGme, which are gen-
349 erally mutually exclusive⁷³. In EpiLCs, loss of KDM5C binding at a subset of germline gene promoters,
350 e.g. *D1Pas1*, strongly impaired promoter CGI methylation and resulted in their long-lasting de-repression
351 into adulthood. Removal of H3K4me2/3 at CGIs is a plausible mechanism for KDM5C-mediated germline
352 gene suppression^{13,54}, given H3K4me2/3 repell DNMT3 activity^{65,66}. However, emerging work indicates
353 many histone-modifying enzymes have non-catalytic functions that influence gene expression, sometimes
354 even more potently than their catalytic roles^{74,75}. Indeed, KDM5C's catalytic activity was recently found to be
355 dispensable for repressing *Dazl* in ESCs⁴⁵. In our study, *Dazl*'s promoter still gained CpGme in *Kdm5c*-KO
356 exEpiLCs, even with elevated H3K4me2. *Dazl* and a few other germline genes employ multiple repressive
357 mechanisms to facilitate CpGme, such as DNMT3A/B recruitment via E2F6 and MGA^{17,18,46,47}. Thus, while
358 some germline CGIs require KDM5C-mediated H3K4me removal to overcome promoter CGI escape from
359 CpGme^{73,76}, others do not. These results also suggest the requirement for KDM5C's catalytic activity can
360 change depending upon the locus and developmental stage. Further experiments are required to determine
361 if catalytically inactive KDM5C can suppress germline genes at later developmental stages.

362 By generating a comprehensive list of mouse germline-enriched genes, we revealed distinct derepressive
363 mechanisms governing early versus late-stage germline programs. Previous work on germline gene silencing
364 has focused on genes with promoter CGIs^{19,73}, and indeed the majority of KDM5C targets in EpiLCs were
365 germ cell identity genes harboring CGIs. However, over 70% of germline-enriched gene promoters lacked
366 CGIs, including the many KDM5C-unbound germline genes that are de-repressed in *Kdm5c*-KO cells. CGI-
367 free, KDM5C-unbound germline genes were primarily late-stage spermatogenesis genes and significantly
368 enriched for RFX2 binding sites, a central regulator of spermiogenesis^{63,64}. These data suggest that once
369 activated during early embryogenesis, drivers of germline gene expression like *Rfx2*, *Stra8*, and *Dazl* turn
370 on downstream germline programs, ultimately culminating in the expression of spermiogenesis genes in
371 the adult *Kdm5c*-KO brain. Therefore, we propose KDM5C is recruited via promoter CGIs to act as a brake
372 against runaway activation of germline-specific programs. Future studies should address how KDM5C is
373 targeted to CGIs.

374 The above work provides the mechanistic foundation for KDM5C-mediated repression of tissue and
375 germline-specific genes. However, the contribution of these ectopic, tissue-specific genes towards neurolog-
376 ical impairments is still unknown. In addition to germline genes, we also identified significant enrichment
377 of muscle and liver-enriched transcripts within the *Kdm5c*-KO brain. Intriguingly, select liver and muscle-
378 enriched DEGs do have known roles within the brain, such as the liver-enriched lipid metabolism gene
379 *Apolipoprotein C-I (Apoc1)*²⁸. *APOC1* dysregulation is implicated in Alzheimer's disease in humans⁷⁷ and
380 overexpression of *Apoc1* in the mouse brain can impair learning and memory⁷⁸. KDM5C may therefore be
381 crucial for neurodevelopment by fine-tuning the expression of tissue-enriched, dosage-sensitive genes like
382 *Apoc1*.

383 Given that germline genes have no known functions within the brain, their impact upon neurodevelopment
384 is currently unknown. In *C. elegans*, somatic misexpression of germline genes via loss of *Retinoblastoma*
385 (*Rb*) homologs results in enhanced piRNA signaling and ectopic P granule formation in neurons^{79,80}. Ectopic
386 testicular germline transcripts have also been observed in a variety of cancers, including brain tumors in
387 *Drosophila* and mammals^{81,82} and shown to promote cancer progression^{83–85}. Intriguingly, mouse models
388 and human cells for other chromatin-linked NDDs also display impaired soma-germline demarcation^{86–88},
389 such as mutations in DNA methyltransferase 3b (DNMT3B), H3K9me1/2 methyltransferases G9A/GLP,
390 and methyl-CpG -binding protein 2 (MECP2). Recently, the transcription factor ZMYM2 (ZNF198), whose
391 mutation causes a NDD (OMIM #619522), was also shown to repress germline genes by promoting H3K4me
392 removal and CpGme⁸⁹. Thus, KDM5C is among a growing cohort of neurodevelopmental disorders with
393 erosion of the germline-soma boundary. Further research is required to determine the impact of these
394 germline genes upon neuronal functions and the extent to which this phenomenon occurs in humans.

395 Materials and Methods

396 Classifying tissue-enriched and germline-enriched genes

397 Tissue-enriched differentially expresssd genes (DEGs) were determined by their classification in a previ-
398 ously published dataset from 17 male and female mouse tissues²³. This study defined tissue expression as
399 greater than 1 Fragments Per Kilobase of transcript per Million mapped read (FPKM) and tissue enrichment
400 as at least 4-fold higher expression than any other tissue.

401 We curated a list of germline-enriched genes using an RNA-seq dataset from wild-type and germline-
402 depleted (*Kit^{W/Wv}*) male and female mouse embryos from embryonic day 12, 14, and 16³², as well as adult
403 male testes²⁹. Germline-enriched genes met the following criteria: 1) their expression is greater than 1
404 FPKM in wild-type germline 2) their expression in any wild-type somatic tissues²³ does not exceed 20%
405 of maximum expression in wild-type germline, and 3) their expression in the germ cell-depleted (*Kit^{W/Wv}*)
406 germline, for any sex or time point, does not exceed 20% of maximum expression in wild-type germline. We

407 defined sperm and egg-biased genes as those whose expression in the opposite sex, at any time point, is no
408 greater than 20% of the gene's maximum expression in a given sex. Genes that did not meet this threshold
409 for either sex were classified as 'unbiased'.

410 **Cell culture**

411 We utilized our previously established cultures of male wild-type and *Kdm5c* knockout (-KO)
412 embryonic stem cells⁴¹. Sex was confirmed by genotyping *Uba1/Uba1y* on the X and Y chromo-
413 somes with the following primers: 5'-TGGATGGTGTGCCAATG-3', 5'-CACCTGCACGTTGCCCTT-
414 3'. Deletion of *Kdm5c* exons 11 and 12, which destabilize KDM5C protein¹², was confirmed
415 through the primers 5'-ATGCCCATATTAAGAGTCCCTG-3', 5'-TCTGCCTTGATGGACTGTT-3', and
416 5'-GGTTCTAACACTCACATAGTG-3'.

417 Embryonic stem cells (ESCs) and epiblast-like cells were cultured using previously established
418 methods³⁷. Briefly, ESCs were initially cultured in primed ESC (pESC) media consisting of KnockOut
419 DMEM (Gibco#10829–018), fetal bovine serum (Gibco#A5209501), KnockOut serum replacement
420 (Invitrogen#10828–028), Glutamax (Gibco#35050-061), Anti-Anti (Gibco#15240-062), MEM Non-essential
421 amino acids (Gibco#11140-050), and beta-mercaptoethanol (Sigma#M7522). They were then transitioned
422 into ground-state, "naïve" ESCs (nESCs) by culturing for four passages in N2B27 media containing
423 DMEM/F12 (Gibco#11330–032), Neurobasal media (Gibco#21103–049), Gluamax (Gibco#35050-061),
424 Anti-Anti (Gibco#15240-062), N2 supplement (Invitrogen#17502048), and B27 supplement without vitamin
425 A (Invitrogen#12587-010), and beta-mercaptoethanol (Sigma#M7522). Both pESC and nESC media
426 were supplemented with 3 µM GSK3 inhibitor CHIR99021 (Sigma #SML1046-5MG), 1 µM MEK inhibitor
427 PD0325901 (Sigma #PZ0162-5MG), and 1,000 units/mL leukemia inhibitory factor (LIF, Millipore#ESG1107).

428 nESCs were differentiated into epiblast-like cells (EpiLCs, 48 hours) and extendend EpiLCs (exEpiLCs,
429 96 hours) by culturing in N2B27 media containing DMEM/F12, Neurobasal media, Gluamax, Anti-Anti, N2
430 supplement, B27 supplement (Invitrogen#17504044), and beta-mercaptoethanol supplemented with 10
431 ng/mL fibroblast growth factor 2 (FGF2, R&D Biotechne 233-FB), and 20 ng/mL activin A (R&D Biotechne
432 338AC050CF), as previously described³⁷.

433 **Real time quantitative PCR (RT-qPCR)**

434 nESCs were differentiated into EpiLCs as described above. Cells were lysed with Tri-reagent BD (Sigma
435 #T3809) at 0, 24, and 48 hours of differentiation. RNA was phase separated with 0.1 µL/µL 1-bromo-3-
436 chloropropane (Sigma #B9673) and then precipitated with with isopropanol (Sigma #I9516) and ethanol puri-
437 fied. For each sample, 2 µg of RNA was reverse transcribed using the ProtoScript II Reverse transcriptase kit
438 from New England Biolabs (NEB #M0368S) and primed with oligo dT. Expression of *Kdm5c* was detected us-
439 ing the primers 5'-CCCATGGAGGCCAGAGAATAAG-3' 5'-CTCAGCGGATAAGAGAATTGCTAC-3' and nor-

440 malized to TBP using the primers 5'-TTCAGAGGATGCTCTAGGAAAGA-3' 5'-CTGTGGAGTAAGTCCTGTGCC-
441 3' with the Power SYBR™ Green PCR Master Mix (ThermoFisher #4367659).

442 **Western Blot**

443 Total protein was extracted during nESC to EpiLC differentiation at 0, 24, and 48 hours by sonicating cells
444 at 20% amplitude for 15 seconds in 2X SDS sample buffer, then boiling at 100 °C for 10 minutes. Proteins
445 were separated on a 7.5% SDS page gel, transferred overnight onto a fluorescent membrane, blotted for
446 rabbit anti-KDM5C (in house, 1:500) and mouse anti-DAXX (Santa Cruz #(H-7): sc-8043, 1:500), and then
447 imaged using the LiCor Odyssey CLx system. Band intensity was quantified using ImageJ.

448 **RNA sequencing (RNA-seq) data analysis**

449 After ensuring read quality via FastQC (v0.11.8), reads were then mapped to the mm10 *Mus musculus*
450 genome (Gencode) using STAR (v2.5.3a), during which we removed duplicates and kept only uniquely
451 mapped reads. Count files were generated by FeatureCounts (Subread v1.5.0), and BAM files were
452 converted to bigwigs using deeptools (v3.1.3) and visualized by the UCSC genome browser⁶⁸. RStudio
453 (v3.6.0) was then used to analyze counts files by DESeq2 (v1.26.0)²⁴ to identify differentially expressed
454 genes (DEGs) with a q-value (p-adjusted via FDR/Benjamini–Hochberg correction) less than 0.1 and a log2
455 fold change greater than 0.5. For all DESeq2 analyses, log2 fold changes were calculated with IfcShrink
456 using the ashR package⁹⁰. MA-plots were generated by ggpubr (v0.6.0), and Eulerr diagrams were generated
457 by eulerr (v6.1.1). Boxplots and scatterplots were generated by ggpubr (v0.6.0) and ggplot2 (v3.3.2). The
458 Upset plot was generated via the package UpSetR (v1.4.0)⁹¹. Gene ontology (GO) analyses were performed
459 by the R package enrichPlot (v1.16.2) using the biological processes setting and compareCluster.

460 **Chromatin immunoprecipitation followed by DNA sequencing (ChIP-seq) data analysis**

461 ChIP-seq reads were aligned to mm10 using Bowtie1 (v1.1.2) allowing up to two mismatches. Only
462 uniquely mapped reads were used for analysis. Peaks were called using MACS2 software (v2.2.9.1) using
463 input BAM files for normalization, with filters for a q-value < 0.1 and a fold enrichment > 1. We removed
464 “black-listed” genomic regions that often give aberrant signals. Common peak sets were obtained in R via
465 DiffBind⁹² (v3.6.5). In the case of KDM5C ChIP-seq, *Kdm5c*-KO false-positive peaks were then removed from
466 wild-type samples using bedtools (v2.25.0). Peak proximity to genomic loci was determined by ChIPSeeker⁹³
467 (v1.32.1). Gene ontology (GO) analyses were performed by the R package enrichPlot (v1.16.2) using the
468 biological processes setting and compareCluster. Enriched motifs were identified using HOMER⁵⁹ to search
469 for known motifs within 500 base pairs upstream and downstream of the transcription start site. Average binding
470 across genes was visualized using deeptools (v3.1.3). Bigwigs were visualized using the UCSC genome
471 browser⁶⁸.

472 CpG island (CGI) analysis

473 Locations of CpG islands were determined through the mm10 UCSC genome browser CpG island track⁶⁸,
474 which classified CGIs as regions that have greater than 50% GC content, are larger than 200 base pairs,
475 and have a ratio of CG dinucleotides observed over the expected amount greater than 0.6. CGI genomic
476 coordinates were then annotated using ChIPseeker⁹³ (v1.32.1) and filtered for ones that lie within promoters
477 of germline-enriched genes (TSS ± 500).

478 Whole genome bisulfite sequencing (WGBS)

479 Genomic DNA (gDNA) from male naïve ESCs and extended EpiLCs was extracted using the Wizard
480 Genomic DNA Purification Kit (Promega A1120), following the instructions for Tissue Culture Cells. gDNA
481 from two wild-types and two *Kdm5c*-KOs of each cell type was sent to Novogene for WGBS using the
482 Illumina NovaSeq X Plus platform and sequenced for 150 bp paired-end reads (PE150). All samples had
483 greater than 99% bisulfite conversion rates. Reads were adapter and quality trimmed with Trim Galore
484 (v0.6.10) and aligned to the mm10 genome using Bismark⁹⁴ (v0.22.1). Analysis of differential methylation at
485 gene promoters was performed using methylKit⁶⁹ (v1.28.0) with a minimum coverage of 3 paired reads, a
486 percentage greater than 25% or less than -25%, and q-value less than 0.01. methylKit was also used to
487 calculate average percentage methylation at germline gene promoters. Methylation bedgraph tracks were
488 generated via Bismark and visualized using the UCSC genome browser⁶⁸.

489 Data availability

490 WGBS in wild-type and *Kdm5c*-KO ESCs and exEpiLCs

491 Raw fastq files are deposited in the Sequence Read Archive (SRA) <https://www.ncbi.nlm.nih.gov/sra>
492 under the bioProject PRJNA1165148. <https://www.ncbi.nlm.nih.gov/bioproject/PRJNA1165148>

493 Published datasets

494 All published datasets are available at the Gene Expression Omnibus (GEO) <https://www.ncbi.nlm.nih.gov/geo/>. Published RNA-seq datasets analyzed in this study included the male wild-type and *Kdm5c*-KO
495 adult amygdala and hippocampus²², available at GEO: GSE127722. Male and female wild-type, *Kdm5c*-KO,
496 and *Kdm5c*-HET EpiLCs⁴¹ are available at GEO: GSE96797.

498 Previously published ChIP-seq experiments included KDM5C binding in wild-type and *Kdm5c*-KO
499 EpiLCs⁴¹ (available at GEO: GSE96797) and mouse primary neuron cultures (PNCs) from the cortex
500 and hippocampus¹² (available at GEO: GSE61036). ChIP-seq of histone 3 lysine 4 dimethylation (H3K4me2)
501 in male wild-type and *Kdm5c*-KO EpiLCs⁴¹ is also available at GEO: GSE96797. ChIP-seq of histone 3 lysine
502 4 trimethylation (H3K4me3) in wild-type and *Kdm5c*-KO male amygdala²² are available at GEO: GSE127817.

503 **Data analysis**

504 Scripts used to generate the results, tables, and figures of this study are available via the GitHub
505 repository: https://github.com/kbonefas/KDM5C_Germ_Mechanism

506 **Acknowledgements**

507 We thank Drs. Sundeep Kalantry, Milan Samanta, and Rebecca Malcore for providing protocols and
508 expertise in culturing mouse ESCs and EpiLCs, as well as providing the wild-type and *Kdm5c*-KO ESCs
509 used in this study. We thank Dr. Jacob Mueller for his insight in germline gene regulation and directing
510 us to the germline-depleted mouse models. We also thank Drs. Gabriel Corfas, Kenneth Kwan, Natalie
511 Tronson, Michael Sutton, Stephanie Bielas, Donna Martin, and the members of the Iwase, Sutton, Bielas,
512 and Martin labs for helpful discussions and critiques of the data. We thank members of the University
513 of Michigan Reproductive Sciences Program for providing feedback throughout the development of this
514 work. This work was supported by grants from the National Institutes of Health (NIH) National Institute of
515 Neurological Disorders and Stroke (NS089896, 5R21NS104774, and NS116008 to S.I.), National Institute
516 of Mental Health (1R21MH135290 to S.I.), the Simons Foundation Autism Research Initiative (SFARI, SFI-
517 AN-AR-Pilot-00005721 to S.I.), the Farrehi Family Foundation Grant (to S.I.), the University of Michigan
518 Career Training in Reproductive Biology (NIH T32HD079342, to K.M.B.), the NIH Early Stage Training in
519 the Neurosciences Training Grant (NIH T32NS076401 to K.M.B.), and the Michigan Predoctoral Training in
520 Genetics Grant (NIH T32GM007544, to I.V.)

521 **Author Contributions**

522 K.M.B. and S.I. conceived the study and designed the experiments. I.V. generated the ESC and exEpiLC
523 WGBS data. K.M.B performed all data analysis and all other experiments. The manuscript was written by
524 K.M.B and S.I., and edited by K.M.B, S.I., and I.V.

525 **Declaration of Interest**

526 S.I. is a member of the Scientific Advisory Board of KDM5C Advocacy, Research, Education & Support
527 (KARES). Other authors declare no conflict of interest.

528 **References**

- 529 1. Strahl, B.D., and Allis, C.D. (2000). The language of covalent histone modifications. *Nature* **403**,
530 41–45. <https://doi.org/10.1038/47412>.
- 531 2. Jenuwein, T., and Allis, C.D. (2001). Translating the Histone Code. *Science* **293**, 1074–1080.
532 <https://doi.org/10.1126/science.1063127>.
- 533 3. Lewis, E.B. (1978). A gene complex controlling segmentation in *Drosophila*. *Nature* **276**, 565–570.
534 <https://doi.org/10.1038/276565a0>.
- 535 4. Kennison, J.A., and Tamkun, J.W. (1988). Dosage-dependent modifiers of polycomb and antennapedia
536 mutations in *Drosophila*. *Proc. Natl. Acad. Sci. U.S.A.* **85**, 8136–8140. <https://doi.org/10.1073/pnas.8>
537 5.21.8136.
- 538 5. Kassis, J.A., Kennison, J.A., and Tamkun, J.W. (2017). Polycomb and Trithorax Group Genes in
539 *Drosophila*. *Genetics* **206**, 1699–1725. <https://doi.org/10.1534/genetics.115.185116>.
- 540 6. Gabriele, M., Lopez Tobon, A., D'Agostino, G., and Testa, G. (2018). The chromatin basis of
541 neurodevelopmental disorders: Rethinking dysfunction along the molecular and temporal axes. *Prog
542 Neuropsychopharmacol Biol Psychiatry* **84**, 306–327. <https://doi.org/10.1016/j.pnpbp.2017.12.013>.
- 543 7. Schaefer, A., Sampath, S.C., Intrator, A., Min, A., Gertler, T.S., Surmeier, D.J., Tarakhovsky, A.,
544 and Greengard, P. (2009). Control of cognition and adaptive behavior by the GLP/G9a epigenetic
545 suppressor complex. *Neuron* **64**, 678–691. <https://doi.org/10.1016/j.neuron.2009.11.019>.
- 546 8. Iwase, S., Lan, F., Bayliss, P., De La Torre-Ubieta, L., Huarte, M., Qi, H.H., Whetstine, J.R., Bonni, A.,
547 Roberts, T.M., and Shi, Y. (2007). The X-Linked Mental Retardation Gene SMCX/JARID1C Defines a
548 Family of Histone H3 Lysine 4 Demethylases. *Cell* **128**, 1077–1088. <https://doi.org/10.1016/j.cell.200>
7.02.017.
- 549 9. Claes, S., Devriendt, K., Van Goethem, G., Roelen, L., Meireleire, J., Raeymaekers, P., Cassiman,
550 J.J., and Fryns, J.P. (2000). Novel syndromic form of X-linked complicated spastic paraparesia. *Am J
Med Genet* **94**, 1–4.
- 551 10. Jensen, L.R., Amende, M., Gurok, U., Moser, B., Gimmel, V., Tzschach, A., Janecke, A.R., Tariverdian,
552 G., Chelly, J., Fryns, J.P., et al. (2005). Mutations in the JARID1C gene, which is involved in
553 transcriptional regulation and chromatin remodeling, cause X-linked mental retardation. *Am J Hum
554 Genet* **76**, 227–236. <https://doi.org/10.1086/427563>.
- 555 11. Carmignac, V., Nambot, S., Lehalle, D., Callier, P., Moortgat, S., Benoit, V., Ghoumid, J., Delobel,
556 B., Smol, T., Thuillier, C., et al. (2020). Further delineation of the female phenotype with KDM5C
557 disease causing variants: 19 new individuals and review of the literature. *Clin Genet* **98**, 43–55.
558 <https://doi.org/10.1111/cge.13755>.

- 551 12. Iwase, S., Brookes, E., Agarwal, S., Badeaux, A.I., Ito, H., Vallianatos, C.N., Tomassy, G.S., Kasza, T.,
Lin, G., Thompson, A., et al. (2016). A Mouse Model of X-linked Intellectual Disability Associated with
Impaired Removal of Histone Methylation. *Cell Reports* *14*, 1000–1009. <https://doi.org/10.1016/j.celrep.2015.12.091>.
- 552
- 553 13. Scandaglia, M., Lopez-Atalaya, J.P., Medrano-Fernandez, A., Lopez-Cascales, M.T., Del Blanco, B.,
Lipinski, M., Benito, E., Olivares, R., Iwase, S., Shi, Y., et al. (2017). Loss of Kdm5c Causes Spurious
Transcription and Prevents the Fine-Tuning of Activity-Regulated Enhancers in Neurons. *Cell Rep* *21*,
47–59. <https://doi.org/10.1016/j.celrep.2017.09.014>.
- 554
- 555 14. Bonefas, K.M., Vallianatos, C.N., Raines, B., Tronson, N.C., and Iwase, S. (2023). Sexually Dimorphic
Alterations in the Transcriptome and Behavior with Loss of Histone Demethylase KDM5C. *Cells* *12*,
637. <https://doi.org/10.3390/cells12040637>.
- 556
- 557 15. Devlin, D.K., Ganley, A.R.D., and Takeuchi, N. (2023). A pan-metazoan view of germline-soma
distinction challenges our understanding of how the metazoan germline evolves. *Current Opinion in
Systems Biology* *36*, 100486. <https://doi.org/10.1016/j.coisb.2023.100486>.
- 558
- 559 16. Lehmann, R. (2012). Germline Stem Cells: Origin and Destiny. *Cell Stem Cell* *10*, 729–739.
<https://doi.org/10.1016/j.stem.2012.05.016>.
- 560
- 561 17. Endoh, M., Endo, T.A., Shinga, J., Hayashi, K., Farcas, A., Ma, K.W., Ito, S., Sharif, J., Endoh, T.,
Onaga, N., et al. (2017). PCGF6-PRC1 suppresses premature differentiation of mouse embryonic
stem cells by regulating germ cell-related genes. *eLife* *6*. <https://doi.org/10.7554/eLife.21064>.
- 562
- 563 18. Mochizuki, K., Sharif, J., Shirane, K., Uranishi, K., Bogutz, A.B., Janssen, S.M., Suzuki, A., Okuda,
A., Koseki, H., and Lorincz, M.C. (2021). Repression of germline genes by PRC1.6 and SETDB1
in the early embryo precedes DNA methylation-mediated silencing. *Nat Commun* *12*, 7020. <https://doi.org/10.1038/s41467-021-27345-x>.
- 564
- 565 19. Borgel, J., Guibert, S., Li, Y., Chiba, H., Schübeler, D., Sasaki, H., Forné, T., and Weber, M. (2010).
Targets and dynamics of promoter DNA methylation during early mouse development. *Nat Genet* *42*,
1093–1100. <https://doi.org/10.1038/ng.708>.
- 566
- 567 20. Velasco, G., Hubé, F., Rollin, J., Neuillet, D., Philippe, C., Bouzinba-Segard, H., Galvani, A., Viegas-
Péquignot, E., and Francastel, C. (2010). Dnmt3b recruitment through E2F6 transcriptional repressor
mediates germ-line gene silencing in murine somatic tissues. *Proc Natl Acad Sci U S A* *107*, 9281–
9286. <https://doi.org/10.1073/pnas.1000473107>.
- 568
- 569 21. Hackett, J.A., Reddington, J.P., Nestor, C.E., Dunican, D.S., Branco, M.R., Reichmann, J., Reik,
W., Surani, M.A., Adams, I.R., and Meehan, R.R. (2012). Promoter DNA methylation couples
genome-defence mechanisms to epigenetic reprogramming in the mouse germline. *Development*
139, 3623–3632. <https://doi.org/10.1242/dev.081661>.
- 570

- 571 22. Vallianatos, C.N., Raines, B., Porter, R.S., Bonefas, K.M., Wu, M.C., Garay, P.M., Collette, K.M.,
Seo, Y.A., Dou, Y., Keegan, C.E., et al. (2020). Mutually suppressive roles of KMT2A and KDM5C
in behaviour, neuronal structure, and histone H3K4 methylation. *Commun Biol* 3, 278. <https://doi.org/10.1038/s42003-020-1001-6>.
- 572
- 573 23. Li, B., Qing, T., Zhu, J., Wen, Z., Yu, Y., Fukumura, R., Zheng, Y., Gondo, Y., and Shi, L. (2017). A
Comprehensive Mouse Transcriptomic BodyMap across 17 Tissues by RNA-seq. *Sci Rep* 7, 4200.
<https://doi.org/10.1038/s41598-017-04520-z>.
- 574
- 575 24. Love, M.I., Huber, W., and Anders, S. (2014). Moderated estimation of fold change and dispersion for
576 RNA-seq data with DESeq2. *Genome Biol* 15, 550. <https://doi.org/10.1186/s13059-014-0550-8>.
- 577 25. Crackower, M.A., Kolas, N.K., Noguchi, J., Sarao, R., Kikuchi, K., Kaneko, H., Kobayashi, E., Kawai, Y.,
Kozieradzki, I., Landers, R., et al. (2003). Essential Role of Fkbp6 in Male Fertility and Homologous
578 Chromosome Pairing in Meiosis. *Science* 300, 1291–1295. <https://doi.org/10.1126/science.1083022>.
- 579 26. Xiol, J., Cora, E., Koglgruber, R., Chuma, S., Subramanian, S., Hosokawa, M., Reuter, M., Yang, Z.,
Berninger, P., Palencia, A., et al. (2012). A Role for Fkbp6 and the Chaperone Machinery in piRNA
580 Amplification and Transposon Silencing. *Molecular Cell* 47, 970–979. <https://doi.org/10.1016/j.molcel.2012.07.019>.
- 581 27. Cheng, S., Altmeppen, G., So, C., Welp, L.M., Penir, S., Ruhwedel, T., Menelaou, K., Harasimov, K.,
Stützer, A., Blayney, M., et al. (2022). Mammalian oocytes store mRNAs in a mitochondria-associated
582 membraneless compartment. *Science* 378, eabq4835. <https://doi.org/10.1126/science.abq4835>.
- 583 28. Rouland, A., Masson, D., Lagrost, L., Vergès, B., Gautier, T., and Bouillet, B. (2022). Role of
584 apolipoprotein C1 in lipoprotein metabolism, atherosclerosis and diabetes: A systematic review.
Cardiovasc Diabetol 21, 272. <https://doi.org/10.1186/s12933-022-01703-5>.
- 585 29. Mueller, J.L., Skaletsky, H., Brown, L.G., Zaghlul, S., Rock, S., Graves, T., Auger, K., Warren,
586 W.C., Wilson, R.K., and Page, D.C. (2013). Independent specialization of the human and mouse X
chromosomes for the male germ line. *Nat Genet* 45, 1083–1087. <https://doi.org/10.1038/ng.2705>.
- 587 30. Handel, M.A., and Eppig, J.J. (1979). Sertoli Cell Differentiation in the Testes of Mice Genetically
588 Deficient in Germ Cells. *Biology of Reproduction* 20, 1031–1038. <https://doi.org/10.1095/biolreprod20.5.1031>.
- 589 31. Green, C.D., Ma, Q., Manske, G.L., Shami, A.N., Zheng, X., Marini, S., Moritz, L., Sultan, C.,
Gurczynski, S.J., Moore, B.B., et al. (2018). A Comprehensive Roadmap of Murine Spermatogenesis
Defined by Single-Cell RNA-Seq. *Dev Cell* 46, 651–667.e10. <https://doi.org/10.1016/j.devcel.2018.07.025>.
- 590
- 591 32. Soh, Y.Q., Junker, J.P., Gill, M.E., Mueller, J.L., van Oudenaarden, A., and Page, D.C. (2015). A
Gene Regulatory Program for Meiotic Prophase in the Fetal Ovary. *PLoS Genet* 11, e1005531.
<https://doi.org/10.1371/journal.pgen.1005531>.

- 592
- 593 33. Magnúsdóttir, E., and Surani, M.A. (2014). How to make a primordial germ cell. *Development* *141*,
594 245–252. <https://doi.org/10.1242/dev.098269>.
- 595 34. Günesdogan, U., Magnúsdóttir, E., and Surani, M.A. (2014). Primordial germ cell specification: A
596 context-dependent cellular differentiation event [corrected]. *Philos Trans R Soc Lond B Biol Sci* *369*.
<https://doi.org/10.1098/rstb.2013.0543>.
- 597 35. Bardot, E.S., and Hadjantonakis, A.-K. (2020). Mouse gastrulation: Coordination of tissue patterning,
598 specification and diversification of cell fate. *Mechanisms of Development* *163*, 103617. <https://doi.org/10.1016/j.mod.2020.103617>.
- 599 36. Hayashi, K., Ohta, H., Kurimoto, K., Aramaki, S., and Saitou, M. (2011). Reconstitution of the
600 mouse germ cell specification pathway in culture by pluripotent stem cells. *Cell* *146*, 519–532.
<https://doi.org/10.1016/j.cell.2011.06.052>.
- 601 37. Samanta, M., and Kalantry, S. (2020). Generating primed pluripotent epiblast stem cells: A methodol-
602 ogy chapter. *Curr Top Dev Biol* *138*, 139–174. <https://doi.org/10.1016/bs.ctdb.2020.01.005>.
- 603 38. Welling, M., Chen, H., Muñoz, J., Musheev, M.U., Kester, L., Junker, J.P., Mischerikow, N., Arbab, M.,
604 Kuijk, E., Silberstein, L., et al. (2015). DAZL regulates Tet1 translation in murine embryonic stem cells.
EMBO Reports *16*, 791–802. <https://doi.org/10.15252/embr.201540538>.
- 605 39. Macfarlan, T.S., Gifford, W.D., Driscoll, S., Lettieri, K., Rowe, H.M., Bonanomi, D., Firth, A., Singer, O.,
606 Trono, D., and Pfaff, S.L. (2012). Embryonic stem cell potency fluctuates with endogenous retrovirus
activity. *Nature* *487*, 57–63. <https://doi.org/10.1038/nature11244>.
- 607 40. Suzuki, A., Hirasaki, M., Hishida, T., Wu, J., Okamura, D., Ueda, A., Nishimoto, M., Nakachi, Y.,
608 Mizuno, Y., Okazaki, Y., et al. (2016). Loss of MAX results in meiotic entry in mouse embryonic and
germline stem cells. *Nat Commun* *7*, 11056. <https://doi.org/10.1038/ncomms11056>.
- 609 41. Samanta, M.K., Gayen, S., Harris, C., Maclary, E., Murata-Nakamura, Y., Malcore, R.M., Porter, R.S.,
610 Garay, P.M., Vallianatos, C.N., Samollow, P.B., et al. (2022). Activation of Xist by an evolutionarily
conserved function of KDM5C demethylase. *Nat Commun* *13*, 2602. <https://doi.org/10.1038/s41467-022-30352-1>.
- 611 42. Koubova, J., Menke, D.B., Zhou, Q., Capel, B., Griswold, M.D., and Page, D.C. (2006). Retinoic
acid regulates sex-specific timing of meiotic initiation in mice. *Proc. Natl. Acad. Sci. U.S.A.* *103*,
612 2474–2479. <https://doi.org/10.1073/pnas.0510813103>.
- 613 43. Lin, Y., Gill, M.E., Koubova, J., and Page, D.C. (2008). Germ Cell-Intrinsic and -Extrinsic Factors
614 Govern Meiotic Initiation in Mouse Embryos. *Science* *322*, 1685–1687. <https://doi.org/10.1126/science.1166340>.

- 615 44. Endo, T., Mikedis, M.M., Nicholls, P.K., Page, D.C., and De Rooij, D.G. (2019). Retinoic Acid and Germ
616 Cell Development in the Ovary and Testis. *Biomolecules* 9, 775. <https://doi.org/10.3390/biom9120775>.
- 617 45. Gupta, N., Yakhou, L., Albert, J.R., Azogui, A., Ferry, L., Kirsh, O., Miura, F., Battault, S., Yamaguchi,
618 K., Laisné, M., et al. (2023). A genome-wide screen reveals new regulators of the 2-cell-like cell state.
Nat Struct Mol Biol. <https://doi.org/10.1038/s41594-023-01038-z>.
- 619 46. Pohlers, M., Truss, M., Frede, U., Scholz, A., Strehle, M., Kuban, R.-J., Hoffmann, B., Morkel, M.,
620 Birchmeier, C., and Hagemeyer, C. (2005). A Role for E2F6 in the Restriction of Male-Germ-Cell-
Specific Gene Expression. *Current Biology* 15, 1051–1057. <https://doi.org/10.1016/j.cub.2005.04.060>.
- 621 47. Dahlet, T., Truss, M., Frede, U., Al Adhami, H., Bardet, A.F., Dumas, M., Vallet, J., Chicher, J.,
622 Hammann, P., Kottnik, S., et al. (2021). E2F6 initiates stable epigenetic silencing of germline genes
during embryonic development. *Nat Commun* 12, 3582. <https://doi.org/10.1038/s41467-021-23596-w>.
- 623 48. Agulnik, A.I., Mitchell, M.J., Mattei, M.G., Borsani, G., Avner, P.A., Lerner, J.L., and Bishop, C.E.
624 (1994). A novel X gene with a widely transcribed Y-linked homologue escapes X-inactivation in mouse
and human. *Hum Mol Genet* 3, 879–884. <https://doi.org/10.1093/hmg/3.6.879>.
- 625 49. Carrel, L., Hunt, P.A., and Willard, H.F. (1996). Tissue and lineage-specific variation in inactive
626 X chromosome expression of the murine Smcx gene. *Hum Mol Genet* 5, 1361–1366. <https://doi.org/10.1093/hmg/5.9.1361>.
- 627 50. Sheardown, S., Norris, D., Fisher, A., and Brockdorff, N. (1996). The mouse Smcx gene exhibits
developmental and tissue specific variation in degree of escape from X inactivation. *Hum Mol Genet*
628 5, 1355–1360. <https://doi.org/10.1093/hmg/5.9.1355>.
- 629 51. Xu, J., Deng, X., and Disteche, C.M. (2008). Sex-Specific Expression of the X-Linked Histone
630 Demethylase Gene Jarid1c in Brain. *PLoS ONE* 3, e2553. <https://doi.org/10.1371/journal.pone.0002553>.
- 631 52. Wang, P.J., McCarrey, J.R., Yang, F., and Page, D.C. (2001). An abundance of X-linked genes
632 expressed in spermatogonia. *Nat Genet* 27, 422–426. <https://doi.org/10.1038/86927>.
- 633 53. Khil, P.P., Smirnova, N.A., Romanienko, P.J., and Camerini-Otero, R.D. (2004). The mouse X
chromosome is enriched for sex-biased genes not subject to selection by meiotic sex chromosome
634 inactivation. *Nat Genet* 36, 642–646. <https://doi.org/10.1038/ng1368>.
- 635 54. Al Adhami, H., Vallet, J., Schaal, C., Schumacher, P., Bardet, A.F., Dumas, M., Chicher, J., Hammann,
636 P., Daujat, S., and Weber, M. (2023). Systematic identification of factors involved in the silencing
of germline genes in mouse embryonic stem cells. *Nucleic Acids Research* 51, 3130–3149. <https://doi.org/10.1093/nar/gkad071>.

- 637 55. Hurlin, P.J. (1999). Mga, a dual-specificity transcription factor that interacts with Max and contains a
T-domain DNA-binding motif. *The EMBO Journal* *18*, 7019–7028. <https://doi.org/10.1093/emboj/18.2.4.7019>.
- 638 56. Stielow, B., Finkernagel, F., Stiewe, T., Nist, A., and Suske, G. (2018). MGA, L3MBTL2 and E2F6
determine genomic binding of the non-canonical Polycomb repressive complex PRC1.6. *PLoS Genet*
640 *14*, e1007193. <https://doi.org/10.1371/journal.pgen.1007193>.
- 641 57. Tatsumi, D., Hayashi, Y., Endo, M., Kobayashi, H., Yoshioka, T., Kiso, K., Kanno, S., Nakai, Y., Maeda,
I., Mochizuki, K., et al. (2018). DNMTs and SETDB1 function as co-repressors in MAX-mediated
repression of germ cell-related genes in mouse embryonic stem cells. *PLoS ONE* *13*, e0205969.
642 <https://doi.org/10.1371/journal.pone.0205969>.
- 643 58. Tahiliani, M., Mei, P., Fang, R., Leonor, T., Rutenberg, M., Shimizu, F., Li, J., Rao, A., and Shi, Y.
(2007). The histone H3K4 demethylase SMCX links REST target genes to X-linked mental retardation.
644 *Nature* *447*, 601–605. <https://doi.org/10.1038/nature05823>.
- 645 59. Heinz, S., Benner, C., Spann, N., Bertolino, E., Lin, Y.C., Laslo, P., Cheng, J.X., Murre, C., Singh, H.,
and Glass, C.K. (2010). Simple Combinations of Lineage-Determining Transcription Factors Prime
cis-Regulatory Elements Required for Macrophage and B Cell Identities. *Molecular Cell* *38*, 576–589.
646 <https://doi.org/10.1016/j.molcel.2010.05.004>.
- 647 60. Gajiwala, K.S., Chen, H., Cornille, F., Roques, B.P., Reith, W., Mach, B., and Burley, S.K. (2000).
Structure of the winged-helix protein hRFX1 reveals a new mode of DNA binding. *Nature* *403*,
648 916–921. <https://doi.org/10.1038/35002634>.
- 649 61. Swoboda, P., Adler, H.T., and Thomas, J.H. (2000). The RFX-Type Transcription Factor DAF-19
Regulates Sensory Neuron Cilium Formation in *C. elegans*. *Molecular Cell* *5*, 411–421. [https://doi.org/10.1016/S1097-2765\(00\)80436-0](https://doi.org/10.1016/S1097-2765(00)80436-0).
- 650 62. Ashique, A.M., Choe, Y., Karlen, M., May, S.R., Phamluong, K., Solloway, M.J., Ericson, J., and
Peterson, A.S. (2009). The Rfx4 Transcription Factor Modulates Shh Signaling by Regional Control of
652 Ciliogenesis. *Sci. Signal.* *2*. <https://doi.org/10.1126/scisignal.2000602>.
- 653 63. Kistler, W.S., Baas, D., Lemeille, S., Paschaki, M., Seguin-Estevez, Q., Barras, E., Ma, W., Duteyrat, J.-
L., Morlé, L., Durand, B., et al. (2015). RFX2 Is a Major Transcriptional Regulator of Spermiogenesis.
654 *PLoS Genet* *11*, e1005368. <https://doi.org/10.1371/journal.pgen.1005368>.
- 655 64. Wu, Y., Hu, X., Li, Z., Wang, M., Li, S., Wang, X., Lin, X., Liao, S., Zhang, Z., Feng, X., et al.
(2016). Transcription Factor RFX2 Is a Key Regulator of Mouse Spermiogenesis. *Sci Rep* *6*, 20435.
656 <https://doi.org/10.1038/srep20435>.
- 657 65. Otani, J., Nankumo, T., Arita, K., Inamoto, S., Ariyoshi, M., and Shirakawa, M. (2009). Structural basis
for recognition of H3K4 methylation status by the DNA methyltransferase 3A ATRX–DNMT3–DNMT3L
domain. *EMBO Reports* *10*, 1235–1241. <https://doi.org/10.1038/embor.2009.218>.

- 658
- 659 66. Guo, X., Wang, L., Li, J., Ding, Z., Xiao, J., Yin, X., He, S., Shi, P., Dong, L., Li, G., et al. (2015).
660 Structural insight into autoinhibition and histone H3-induced activation of DNMT3A. *Nature* **517**,
640–644. <https://doi.org/10.1038/nature13899>.
- 661 67. Meissner, A., Mikkelsen, T.S., Gu, H., Wernig, M., Hanna, J., Sivachenko, A., Zhang, X., Bernstein,
662 B.E., Nusbaum, C., Jaffe, D.B., et al. (2008). Genome-scale DNA methylation maps of pluripotent and
differentiated cells. *Nature* **454**, 766–770. <https://doi.org/10.1038/nature07107>.
- 663 68. Nassar, L.R., Barber, G.P., Benet-Pagès, A., Casper, J., Clawson, H., Diekhans, M., Fischer, C.,
664 Gonzalez, J.N., Hinrichs, A.S., Lee, B.T., et al. (2023). The UCSC Genome Browser database: 2023
update. *Nucleic Acids Research* **51**, D1188–D1195. <https://doi.org/10.1093/nar/gkac1072>.
- 665 69. Akalin, A., Kormaksson, M., Li, S., Garrett-Bakelman, F.E., Figueiroa, M.E., Melnick, A., and Mason,
666 C.E. (2012). methylKit: A comprehensive R package for the analysis of genome-wide DNA methylation
profiles. *Genome Biol* **13**, R87. <https://doi.org/10.1186/gb-2012-13-10-r87>.
- 667 70. Torres-Padilla, M.-E. (2020). On transposons and totipotency. *Philos Trans R Soc Lond B Biol Sci*
668 **375**, 20190339. <https://doi.org/10.1098/rstb.2019.0339>.
- 669 71. Yang, M., Yu, H., Yu, X., Liang, S., Hu, Y., Luo, Y., Izsvák, Z., Sun, C., and Wang, J. (2022). Chemical-
induced chromatin remodeling reprograms mouse ESCs to totipotent-like stem cells. *Cell Stem Cell*
670 **29**, 400–418.e13. <https://doi.org/10.1016/j.stem.2022.01.010>.
- 671 72. Zhang, J., Zhang, M., Acampora, D., Vojtek, M., Yuan, D., Simeone, A., and Chambers, I. (2018).
672 OTX2 restricts entry to the mouse germline. *Nature* **562**, 595–599. <https://doi.org/10.1038/s41586-018-0581-5>.
- 673 73. Weber, M., Hellmann, I., Stadler, M.B., Ramos, L., Pääbo, S., Rebhan, M., and Schübeler, D. (2007).
674 Distribution, silencing potential and evolutionary impact of promoter DNA methylation in the human
genome. *Nat Genet* **39**, 457–466. <https://doi.org/10.1038/ng1990>.
- 675 74. Aubert, Y., Egolf, S., and Capell, B.C. (2019). The Unexpected Noncatalytic Roles of Histone Modifiers
in Development and Disease. *Trends in Genetics* **35**, 645–657. <https://doi.org/10.1016/j.tig.2019.06.004>.
- 676 75. Morgan, M.A.J., and Shilatifard, A. (2020). Reevaluating the roles of histone-modifying enzymes
and their associated chromatin modifications in transcriptional regulation. *Nat Genet* **52**, 1271–1281.
677 <https://doi.org/10.1038/s41588-020-00736-4>.
- 678 76. Long, H.K., King, H.W., Patient, R.K., Odom, D.T., and Klose, R.J. (2016). Protection of CpG
islands from DNA methylation is DNA-encoded and evolutionarily conserved. *Nucleic Acids Res* **44**,
680 6693–6706. <https://doi.org/10.1093/nar/gkw258>.

- 681 77. Leduc, V., Jasmin-Bélanger, S., and Poirier, J. (2010). APOE and cholesterol homeostasis in
682 Alzheimer's disease. *Trends in Molecular Medicine* 16, 469–477. <https://doi.org/10.1016/j.molmed.2010.07.008>.
- 683 78. Abildayeva, K., Berbée, J.F.P., Blokland, A., Jansen, P.J., Hoek, F.J., Meijer, O., Lütjohann, D., Gautier,
684 T., Pillot, T., De Vente, J., et al. (2008). Human apolipoprotein C-I expression in mice impairs learning
and memory functions. *Journal of Lipid Research* 49, 856–869. <https://doi.org/10.1194/jlr.M700518JLR200>.
- 685 79. Wang, D., Kennedy, S., Conte, D., Kim, J.K., Gabel, H.W., Kamath, R.S., Mello, C.C., and Ruvkun,
686 G. (2005). Somatic misexpression of germline P granules and enhanced RNA interference in
retinoblastoma pathway mutants. *Nature* 436, 593–597. <https://doi.org/10.1038/nature04010>.
- 687 80. Wu, X., Shi, Z., Cui, M., Han, M., and Ruvkun, G. (2012). Repression of germline RNAi pathways
688 in somatic cells by retinoblastoma pathway chromatin complexes. *PLoS Genet* 8, e1002542. <https://doi.org/10.1371/journal.pgen.1002542>.
- 689 81. Nielsen, A.Y., and Gjerstorff, M.F. (2016). Ectopic Expression of Testis Germ Cell Proteins in Cancer
690 and Its Potential Role in Genomic Instability. *Int J Mol Sci* 17. <https://doi.org/10.3390/ijms17060890>.
- 691 82. Adebayo Babatunde, K., Najafi, A., Salehipour, P., Modarressi, M.H., and Mobasher, M.B. (2017).
692 Cancer/Testis genes in relation to sperm biology and function. *Iranian Journal of Basic Medical
Sciences* 20. <https://doi.org/10.22038/ijbms.2017.9259>.
- 693 83. Janic, A., Mendizabal, L., Llamazares, S., Rossell, D., and Gonzalez, C. (2010). Ectopic expression
694 of germline genes drives malignant brain tumor growth in *Drosophila*. *Science* 330, 1824–1827.
<https://doi.org/10.1126/science.1195481>.
- 695 84. Ghafouri-Fard, S., and Modarressi, M.-H. (2012). Expression of Cancer–Testis Genes in Brain Tumors:
696 Implications for Cancer Immunotherapy. *Immunotherapy* 4, 59–75. <https://doi.org/10.2217/imt.11.145>.
- 697 85. Nin, D.S., and Deng, L.-W. (2023). Biology of Cancer-Testis Antigens and Their Therapeutic Implica-
698 tions in Cancer. *Cells* 12, 926. <https://doi.org/10.3390/cells12060926>.
- 699 86. Bonefas, K.M., and Iwase, S. (2021). Soma-to-germline transformation in chromatin-linked neurode-
700 velopmental disorders? *FEBS J.* <https://doi.org/10.1111/febs.16196>.
- 701 87. Velasco, G., Walton, E.L., Sterlin, D., Héduouin, S., Nitta, H., Ito, Y., Fouyssac, F., Mégarbané, A.,
702 Sasaki, H., Picard, C., et al. (2014). Germline genes hypomethylation and expression define a
molecular signature in peripheral blood of ICF patients: Implications for diagnosis and etiology.
Orphanet J Rare Dis 9, 56. <https://doi.org/10.1186/1750-1172-9-56>.
- 703 88. Walton, E.L., Francastel, C., and Velasco, G. (2014). Dnmt3b Prefers Germ Line Genes and Cen-
704 tromeric Regions: Lessons from the ICF Syndrome and Cancer and Implications for Diseases. *Biology
(Basel)* 3, 578–605. <https://doi.org/10.3390/biology3030578>.

- 705 89. Graham-Paquin, A.-L., Saini, D., Sirois, J., Hossain, I., Katz, M.S., Zhuang, Q.K.-W., Kwon, S.Y.,
Yamanaka, Y., Bourque, G., Bouchard, M., et al. (2023). ZMYM2 is essential for methylation of
germline genes and active transposons in embryonic development. *Nucleic Acids Research*, gkad540.
706 <https://doi.org/10.1093/nar/gkad540>.
- 707 90. Stephens, M. (2016). False discovery rates: A new deal. *Biostat*, kxw041. <https://doi.org/10.1093/biostatistics/kxw041>.
- 709 91. Conway, J.R., Lex, A., and Gehlenborg, N. (2017). UpSetR: An R package for the visualization of
intersecting sets and their properties. *Bioinformatics* 33, 2938–2940. <https://doi.org/10.1093/bioinformatics/btx364>.
- 711 92. Ross-Innes, C.S., Stark, R., Teschendorff, A.E., Holmes, K.A., Ali, H.R., Dunning, M.J., Brown, G.D.,
Gojis, O., Ellis, I.O., Green, A.R., et al. (2012). Differential oestrogen receptor binding is associated
712 with clinical outcome in breast cancer. *Nature* 481, 389–393. <https://doi.org/10.1038/nature10730>.
- 713 93. Yu, G., Wang, L.G., and He, Q.Y. (2015). ChIPseeker: An R/Bioconductor package for ChIP peak
annotation, comparison and visualization. *Bioinformatics* 31, 2382–2383. <https://doi.org/10.1093/bioinformatics/btv145>.
- 715 94. Krueger, F., and Andrews, S.R. (2011). Bismark: A flexible aligner and methylation caller for Bisulfite-
716 Seq applications. *Bioinformatics* 27, 1571–1572. <https://doi.org/10.1093/bioinformatics/btr167>.

717 **Figures and Tables**

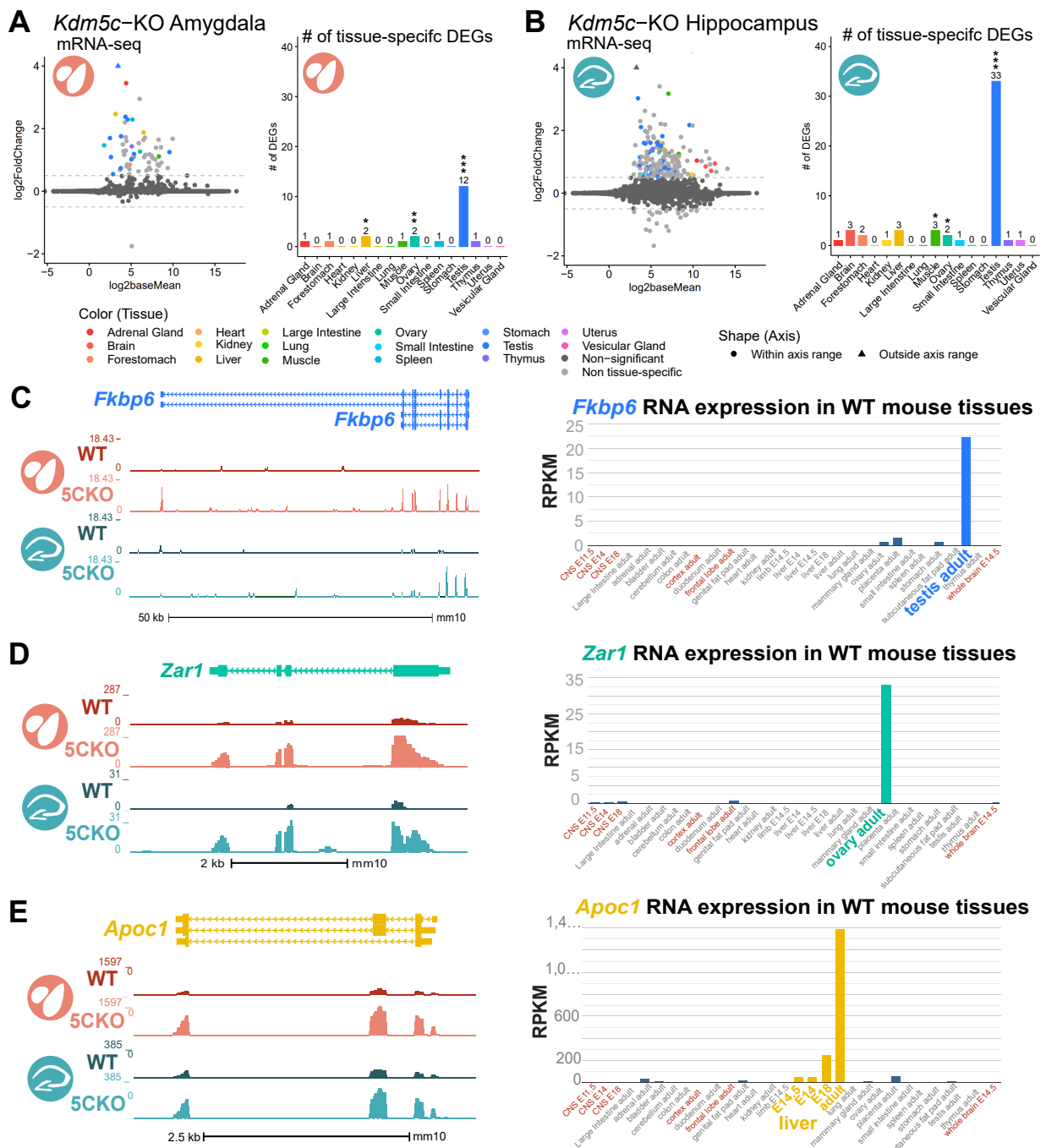


Figure 1: Tissue-enriched genes are misexpressed in the *Kdm5c*-KO brain. **A-B.** Expression of tissue-enriched genes (Li et al 2017) in the male *Kdm5c*-KO amygdala (A) and hippocampus (B). Left - MA plot of mRNA-sequencing. Right - Number of tissue-enriched differentially expressed genes (DEGs). * p<0.05, ** p<0.01, *** p<0.001, Fisher's Exact Test. **C.** Left - UCSC browser view of an example aberrantly expressed testis-enriched DEG, *FK506 binding protein 6* (*Fkbp6*) in the wild-type (WT) and *Kdm5c*-KO (5CKO) amygdala (red) and hippocampus (teal) (Average, n = 4). Right - Expression of *Cyct* in wild-type tissues from NCBI Gene, with testis highlighted in blue and brain tissues highlighted in red. **D.** Left - UCSC browser view of an example ovary-enriched DEG, *Zygotic arrest 1* (*Zar1*). Right - Expression of *Zar1* in wild-type tissues from NCBI Gene, with ovary highlighted in teal and brain tissues highlighted in red. **E.** Left - UCSC browser view of an example liver-enriched DEG, *Apolipoprotein C-I* (*Apoc1*). Right - Expression of *Apoc1* in wild-type tissues from NCBI Gene, with liver highlighted in orange and brain tissues highlighted in red.

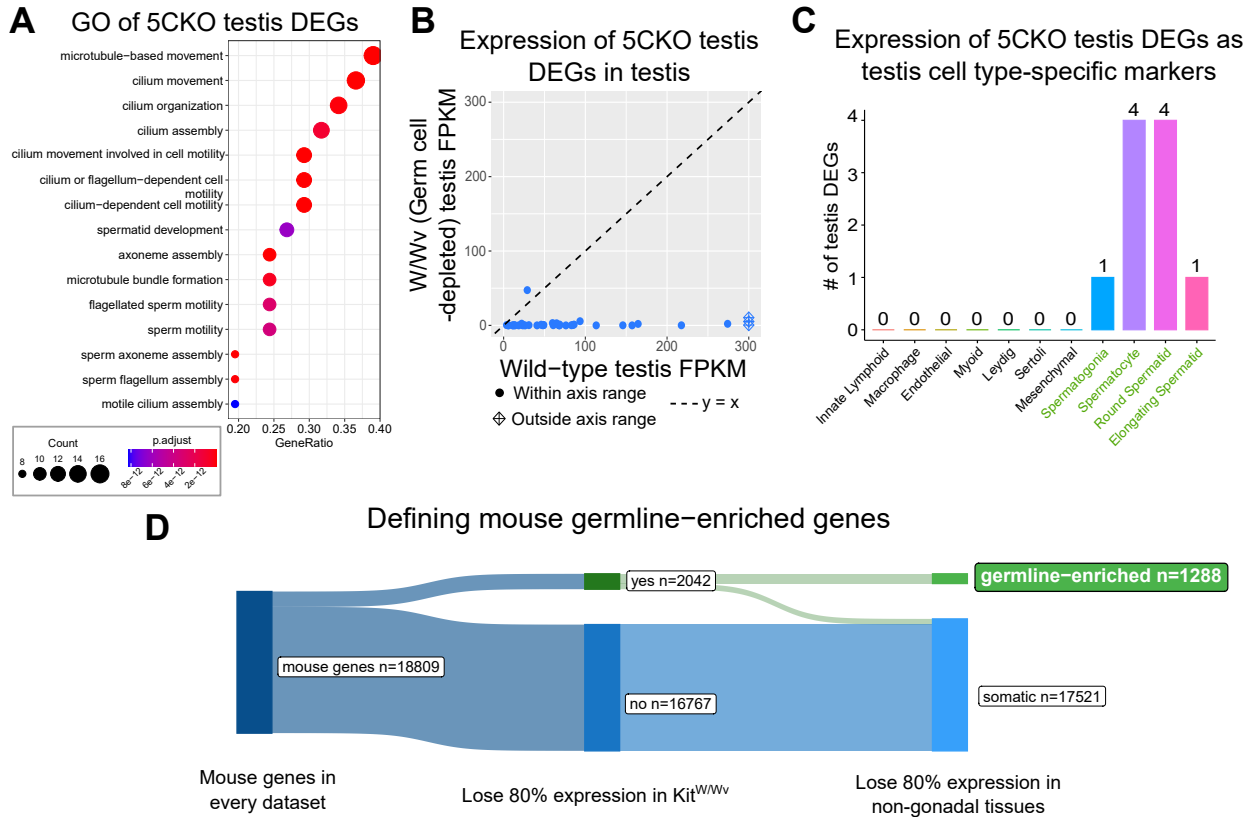


Figure 2: Aberrant transcription of germline genes in the *Kdm5c*-KO in the brain. **A.** enrichPlot gene ontology (GO) of *Kdm5c*-KO amygdala and hippocampus testis-enriched DEGs **B.** Expression of testis DEGs in wild-type (WT) testis versus germ cell-depleted (W/Wv) testis (Mueller et al 2013). Expression is in Fragments Per Kilobase of transcript per Million mapped reads (FPKM). **C.** Number of testis DEGs that were classified as cell-type specific markers in a single cell RNA-seq dataset of the testis (Green et al 2018). Germline cell types are highlighted in green, somatic cell types in black. **D.** Sankey diagram of mouse genes filtered for germline enrichment based on their expression in wild-type and W/Wv mice and in adult mouse non-gonadal tissues (Li et al 2017).

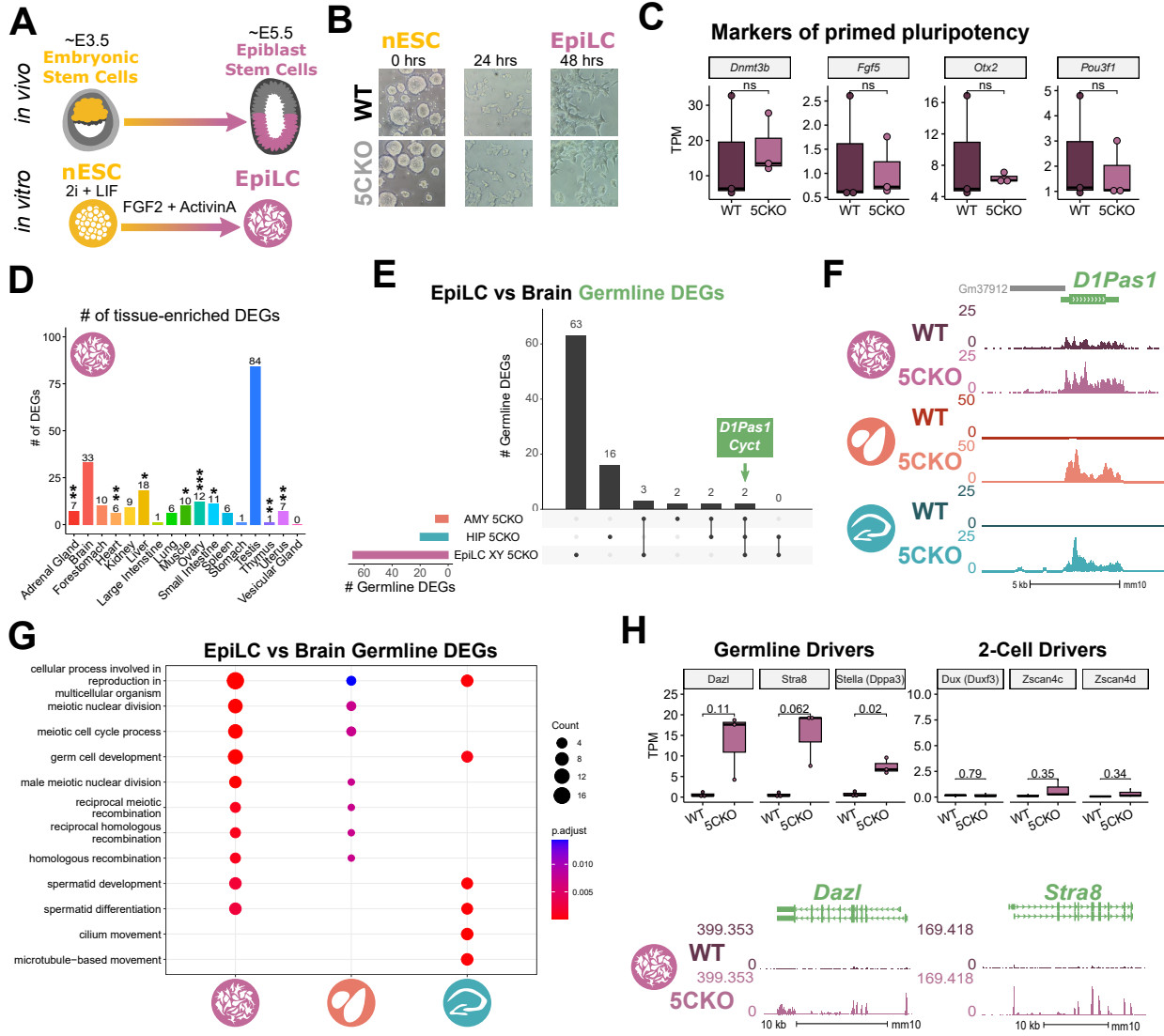


Figure 3: Kdm5c-KO epiblast-like cells express key drivers of germline identity **A.** Top - Diagram of *in vivo* differentiation of embryonic stem cells (ESCs) of the inner cell mass into epiblast stem cells. Bottom - *in vitro* differentiation of ESCs into epiblast-like cells (EpiLCs). **B.** Representative images of male wild-type (WT) and *Kdm5c*-KO (5CKO) cells during ESC to EpiLC differentiation. Brightfield images taken at 20X. **C.** No significant difference in primed pluripotency marker expression in wild-type versus *Kdm5c*-KO EpiLCs. Welch's t-test, expression in transcripts per million (TPM). **D.** Number of tissue-enriched differentially expressed genes (DEGs) in *Kdm5c*-KO EpiLCs. * $p < 0.05$, ** $p < 0.01$, *** $p < 0.001$, Fisher's Exact Test. **E.** Upset plot displaying the overlap of germline DEGs expressed in *Kdm5c*-KO EpiLCs, amygdala (AMY), and hippocampus (HIP) RNA-seq datasets. **F.** UCSC browser view of an example germline gene, *D1Pas1*, that is dysregulated *Kdm5c*-KO EpiLCs (top, purple. Average, $n = 3$), amygdala (middle, red. Average, $n = 4$), and hippocampus (bottom, blue. Average, $n = 4$). **G.** enrichPlot gene ontology analysis comparing enriched biological processes for *Kdm5c*-KO EpiLC, amygdala, and hippocampus germline DEGs. **H.** Top left - Example germline identity DEGs unique to EpiLCs. Top right - Example 2-cell genes that are not dysregulated in *Kdm5c*-KO EpiLCs. p-values for Welch's t-test. Bottom - UCSC browser view of *Dazl* and *Stra8* expression in wild-type and *Kdm5c*-KO EpiLCs (Average, $n = 3$).

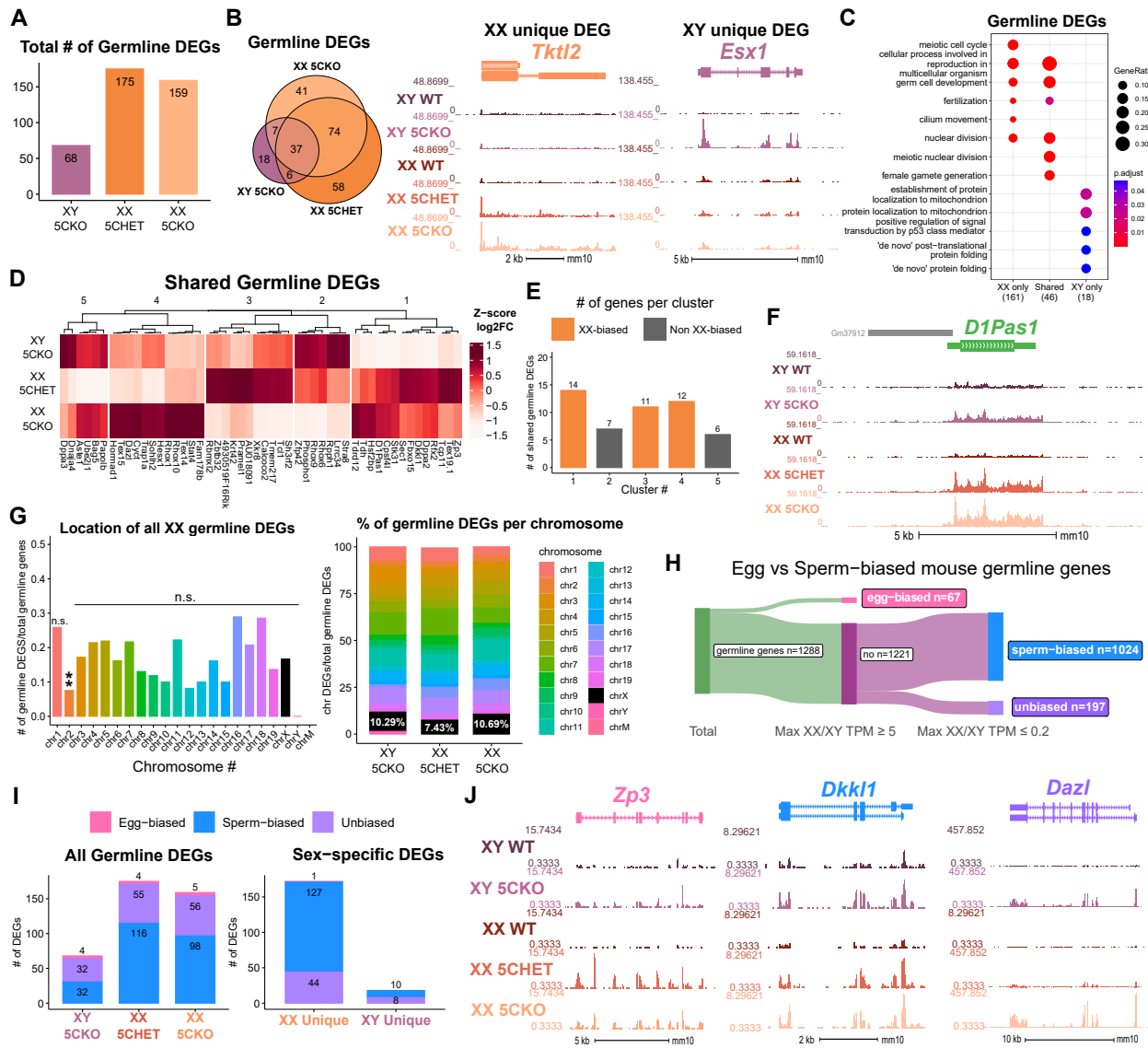


Figure 4: Chromosomal sex influences *Kdm5c*-KO germline gene misexpression. **A.** Total number of germline-enriched RNA-seq DEGs for male hemizygous *Kdm5c* knockout EpiLCs (XY 5CKO, purple), female heterozygous *Kdm5c* knockout (XX 5CHET, orange), female homozygous *Kdm5c* knockout (XX 5CKO, light orange) EpiLCs. **B.** Left - Eulerr overlap of *Kdm5c* mutant male and female EpiLC germline DEGs. Right - Example of germline DEGs unique to females or males, *Tktl2* and *Esx1*. **C.** enrichPlot gene ontology analysis comparing enriched biological processes for germline DEGs shared between *Kdm5c* mutant males and females (Shared), or unique to one sex (XX only or XY only). **D.** Heatmap of germline DEGs shared between male and female mutants. Color is the average log 2 fold change from sex-matched wild-type, z-scored across rows. **E.** Number of genes within each cluster from D. Clusters with higher expression in females compared to males (XX-biased) highlighted in orange. **F.** UCSC browser view of a male and female shared germline DEG *D1Pas1* that is more highly expressed in female mutants (Average, n = 3). **G.** Left - Number of all female germline DEGs located on each chromosome over the total number of germline-enriched genes on that chromosome. P-values for Fisher Exact Test, ** p < 0.01, n.s. non-significant. Germline DEGs were only significant for chromosome 2, in which they were significantly depleted. Right - Percentage of germline DEGs that lie on each chromosome for each *Kdm5c* mutant. X chromosome highlighted in black. **H.** Sankey diagram classifying egg-biased (pink) and sperm-biased (blue) and unbiased (purple) mouse germline-enriched genes. **I.** Number of egg, sperm, or unbiased germline DEGs for male and female *Kdm5c* mutants. **J.** UCSC browser view of egg-biased (*Zp3*), sperm-biased (*Dkk1*), and unbiased (*Dazl*) germline genes dysregulated in both male and female *Kdm5c* mutants (Average of n = 3).

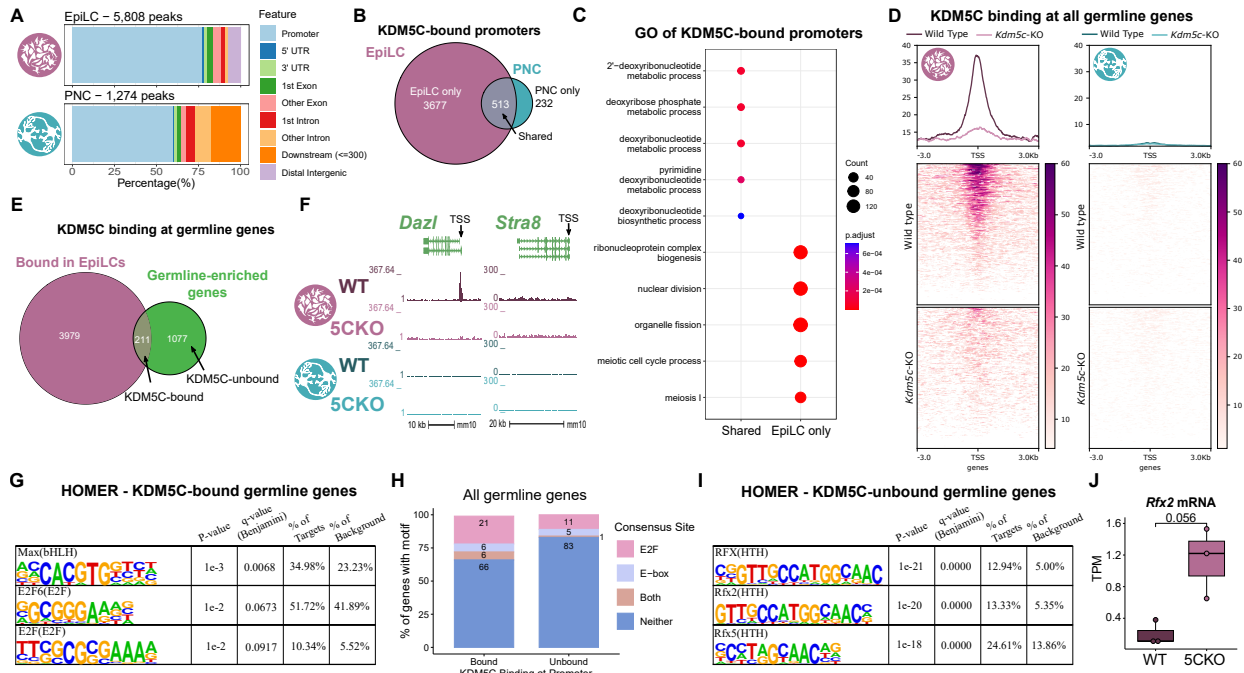


Figure 5: KDM5C binds to a subset of germline gene promoters during early embryogenesis. **A.** ChIPseeker localization of KDM5C peaks at different genomic regions in EpiLCs (top) and hippocampal and cortex primary neuron cultures (PNCs, bottom). **B.** Overlap of genes with KDM5C bound to their promoters ($TSS \pm 500$) in EpiLCs (purple) and PNCs (blue). **C.** Gene ontology (GO) comparison of genes with KDM5C bound to their promoter in EpiLCs and PNCs. Genes were classified as either bound in EpiLCs only (EpiLC only), unique to PNCs (PNC only, no significant ontologies) or bound in both PNCs and EpiLCs (Shared). **D.** Average KDM5C binding around the transcription start site (TSS) of all germline-enriched genes in EpiLCs (left) and PNCs (right). **E.** Eulerr overlap of germline-enriched genes (green) with significant KDM5C binding at their promoter in EpiLCs (purple). **F.** Example KDM5C ChIP-seq signal around the *Dazl* TSS but not *Stra8* in EpiLCs. **G.** HOMER motif analysis of all KDM5C-bound germline gene promoters, highlighting significant enrichment of MAX, E2F6, and E2F motifs. **H.** Number of all gene promoters bound or unbound by KDM5C with instances of the E2F or E-box consensus sequence. **I.** HOMER motif analysis of all KDM5C-unbound germline gene promoters, highlighting significant enrichment of RFX family transcription factor motifs. **J.** Expression of RNA-seq DEG *Rfx2* in wild-type and *Kdm5c*-KO EpiLCs. P-value of Welch's t-test, expression in transcripts per million (TPM).

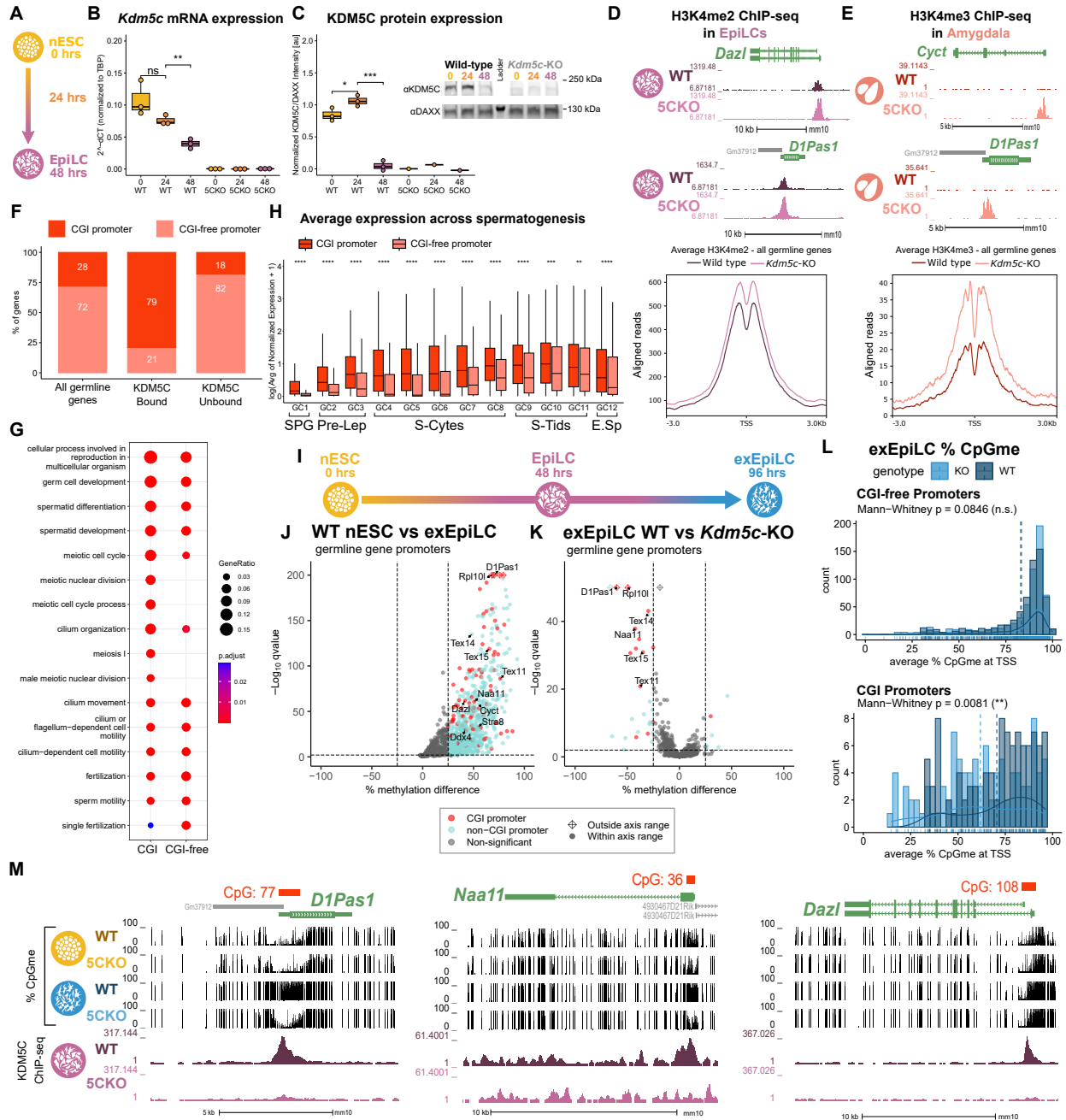


Figure 6: KDM5C promotes long-term silencing of germline genes via DNA methylation at CpG islands. **A.** Diagram of embryonic stem cell (ESC) to epiblast-like cell (EpiLC) differentiation and collection time points. **B.** Real time quantitative PCR (RT-qPCR) of *Kdm5c* mRNA expression in wild-type (WT) and *Kdm5c*-KO (5CKO) ESCs at 0, 24, and 48 hours of differentiation into EpiLCs. Expression calculated in comparison to TBP mRNA expression ($2^{-\Delta\Delta CT}$). * $p < 0.05$, ** $p < 0.01$, *** $p < 0.001$, Welch's t-test. **C.** KDM5C protein expression normalized to DAXX. Quantified intensity using ImageJ (artificial units - au). Right - representative lanes of Western blot for KDM5C and DAXX. * $p < 0.05$, ** $p < 0.01$, *** $p < 0.001$, Welch's t-test. **D.** Top - Representative UCSC browser view of histone 3 lysine 4 dimethylation (H3K4me2) ChIP-seq signal at two germline genes in wild-type and *Kdm5c*-KO EpiLCs. Bottom - Average H3K4me2 signal at the TSS of all germline-enriched genes in wild-type (dark purple) and *Kdm5c*-KO (light purple) EpiLCs. **E.** Top - Representative UCSC browser view of histone 3 lysine 4 trimethylation (H3K4me3) ChIP-seq signal at two germline genes in the wild-type (WT) and *Kdm5c*-KO (5CKO) adult amygdala. Bottom - Average H3K4me3 signal at the transcription start site (TSS) of all germline-enriched genes in wild-type (dark red) and *Kdm5c*-KO (light red) amygdala. **F.** Percentage of germline genes that harbor CpG islands (CGIs) in their promoters (CGI promoter, red), based on UCSC annotation. Left - percentage of all germline-enriched genes, middle - KDM5C-bound germline genes, and right - KDM5C-unbound germline genes. (Legend continued on next page.)

Figure 6: KDM5C promotes long-term silencing of germline genes via DNA methylation at CpG islands. (Legend continued.) **G.** enrichPlot gene ontology analysis of germline genes with (CGI-promoter) or without (CGI-free) CGIs in their promoter. **H.** Expression of germline genes with (CGI-promoter, red) or without (CGI-free, salmon) CGIs in their promoter across stages of spermatogenesis from Green et al 2018. SPG - spermatogonia, Pre-Lep - preleptotene spermatocytes, S-Cytes - meiotic spermatocytes, S-Tids - post-meiotic haploid round spermatids, E.Sp - elongating spermatids. Wilcoxon test, * $p < 0.05$, ** $p < 0.01$, *** $p < 0.001$, **** $p < 0.0001$. **I.** Diagram of ESC to extended EpiLC (exEpiLC) differentiation. **J.** Volcano plot of whole genome bisulfite sequencing (WGBS) comparing CpG methylation (CpGme) at germline gene promoters ($TSS \pm 500$) in wild-type (WT) ESCs versus exEpiLCs. Significantly differentially methylated promoters ($q < 0.01$, $|methylated difference| > 25\%$) with CGIs in red, CGI-free promoters in light blue **K.** Volcano plot of WGBS of wild-type (WT) versus *Kdm5c*-KO exEpiLCs for germline gene promoters. Promoters with CGIs in red, CGI-free promoters in light blue. **L.** Histogram of average percent CpGme at the promoter of germline genes with or without CGIs. Wild-type in navy and *Kdm5c*-KO (KO) in light blue. Dashed lines are average methylation for each genotype, p-values for Mann-Whitney U test. **M.** UCSC browser view of germline genes, showing UCSC annotated CGI with number of CpGs, representative CpGme in wild-type (WT) and *Kdm5c*-KO (5CKO) ESCs and exEpiLCs, and KDM5C ChIP-seq signal in EpiLCs.